

# Observed relationship between CO 2-1 and dust emission during post-AGB phase.<sup>1</sup>

J. H. He<sup>1</sup>, R. Szczerba<sup>2</sup>, T. I. Hasegawa<sup>3</sup>, and M. R. Schmidt<sup>2</sup>  
 jinhuahe@ynao.ac.cn

## ABSTRACT

A CO 2-1 line survey is performed toward a sample of 58 high Galactic latitude post-AGB (pAGB) stars. To complement the observations, a compilation of literature CO 2-1 line data of known pAGB stars is done. After combining the datasets, CO 2-1 line data are available for 133 pAGB stars (about 34 per cent of known pAGB stars) among which 44 are detections. The CO line strengths are compared with infrared dust emission for these pAGB stars by defining a ratio between the integrated CO 2-1 line flux and *IRAS* 25 $\mu$ m flux density (CO-IR ratio). The relationship between the CO-IR ratio and the *IRAS* color C23 (defined with the 25 and 60 $\mu$ m flux densities) is called here the CO-IR diagram. The pAGB objects are found to be located between AGB stars and planetary nebulae (PNe), and segregate into three distinctive groups (I, II and III) on the CO-IR diagram. By analyzing their various properties such as chemical types, spectral types, binarity, circumstellar envelope expansion velocities, and pAGB sub-types on the CO-IR diagram, it is argued that the group-I objects are mainly intermediate mass C-rich pAGB stars in early pAGB stage (almost all of the considered carbon rich ‘21 $\mu$ m’ stars belong to this group); the group-II objects are massive or intermediate mass pAGB stars which already follow the profound trend of PNe; and the group-III objects are mainly low mass binary pAGB stars with very weak CO 2-1 line emission (almost all of the considered RV Tau variables belong to this group). The CO-IR diagram is proven to be a powerful tool to investigate the co-evolution of circumstellar gas and dust during the short pAGB stage of stellar evolution.

*Subject headings:* stars: AGB and post-AGB — (stars:) circumstellar matter — stars: mass-loss — (ISM:) planetary nebulae: general — infrared: stars — radio lines: stars

## 1. INTRODUCTION

After the super-wind has ceased, the evolution of the remnant circumstellar envelope (CSE) around a single post-Asymptotic Giant Branch (post-AGB, or pAGB) star is dominated first by its expansion, and later by photochemical pro-

cesses when the central star temperature quickly rises up. The expansion of the remnant CSE produces a detached circumstellar shell and the object is usually characterized by a double peak spectral energy distribution (SED) due to the lack of hot dust (Kwok 1993). CO molecules in the CSE are protected from photodissociation mainly by self-shielding and line shielding by atomic and molecular H<sub>2</sub> (see e.g., Mamon et al. 1988).

There have been few dedicated works on the relationship between dust and CO in pAGB stars. Alcolea & Bujarrabal (1991) had noticed that some pAGB stars of RV Tauri type are usually very deficient in CO line emission and proposed peculiar elemental abundances that prevent the formation of CO molecules as the possible inter-

<sup>1</sup>Key Laboratory for the Structure and Evolution of Celestial Objects, Yunnan Observatories, Chinese Academy of Sciences, P.O. Box 110, Kunming, Yunnan Province, PR China

<sup>2</sup>N. Copernicus Astronomical Center, Rabianska 8, 87-100 Torun, POLAND

<sup>3</sup>Academia Sinica, Institute of Astronomy and Astrophysics, P.O. Box 23-141, Taipei 10617

<sup>1</sup>The observation project was funded by Academia Sinica, Institute of Astronomy and Astrophysics, Taiwan

pretation of the phenomenon. Bujarrabal et al. (1992) observed  $^{12}\text{CO}$  and  $^{13}\text{CO}$  1-0, 2-1 lines toward several young pAGB stars. Combined with literature data, their results revealed a correlation between CO 1-0 integrated intensity and *IRAS* 60  $\mu\text{m}$  ( $F_{60}$ ) flux density. However, there are some exceptional pAGB stars that show either too strong or too weak CO 1-0 line intensities relative to  $F_{60}$  flux densities. They also noticed the trend that the CO line is stronger in some AGB carbon stars than in investigated pAGB stars. They compared the CO line of the young pAGB stars with other pAGB stars from literature and tentatively concluded that younger pAGB stars might have stronger CO lines. With more observational CO data accumulated to date, it is possible to extend such studies in a more systematic way.

Here we present a new observational study of relationship between dust and CO in the evolving circumstellar envelopes of pAGB objects using the compilation of such objects from the Torun Catalog of pAGB stars (Szczerba et al. 2007, 2012). After description of our observations and data reduction in Sect. 2, the results are presented in Sect. 3. To augment the data set for analysis, we have also performed as complete as possible compilation of literature CO 2-1 data for all known pAGB stars in Sect. 4 (with details presented in the Appendix). Then, the observed relation between the integrated CO 2-1 line fluxes and IR dust emission flux densities is investigated and compared to that of AGB stars and PNe in Sect. 5. To better understand the observed relationship between CO and dust emission, some other properties of the pAGB stars, such as CSE chemical types, spectral types, binarity, spectral energy distribution types, CSE expansion velocities and pAGB sub-types, are discussed in Sect. 6. At the end, the main points of this work are summarized in Sect. 7.

## 2. SAMPLE SELECTION, NEW OBSERVATION AND DATA REDUCTION

In order to explore the relationship between dust and CO in the pAGB circumstellar envelopes with smaller contamination from interstellar CO emission, a sample of 58 high Galactic latitude pAGB stars (with  $|b| \geq 15^\circ$ ) that are acces-

sible from the Arizona Radio Observatory 10 m submillimetre telescope (AROSMT, for objects with a declination  $\geq -38^\circ$ ) were selected from the Torun Catalog of pAGB stars (Szczerba et al. 2007). However, the discussions in this paper will be based on the second version of the catalogue (Szczerba et al. 2012)<sup>2</sup>. We note that, although great efforts have been made in building the catalog, the evolutionary status of some objects (such as RV Tau type and R CrB stars) is still uncertain in the catalog. Almost all of these pAGB objects have optical and/or infrared photometry and/or spectroscopy data, which provides a reliable basis for the analysis in this work.

The ALMA band-6 sideband-separating receiver on the AROSMT telescope was used for our  $^{12}\text{CO}$  J=2-1 line survey from 2007 November to 2008 April. Sky subtraction was made by beam-switch mode with a 2 arcmin throw at 1 Hz wobbling in the azimuth direction. Two filter banks (FFBs, 1 GHz width, 1024 channels) were used for the two linear polarizations. The beam width was about  $32''$  in this line. A nominal factor of 44.4 Jy/K can be used to derive line peak fluxes.

The GILDAS/CLASS package was used to reduce and analyze the data. The two polarizations were combined to improve the S/N. An on-plus-off integration time of 20 min per object yielded an typical root mean square (RMS) of about 15 mK at a spectral resolution of 1 MHz in the polarization-averaged spectral baseline. A linear baseline was removed from each spectrum.

## 3. RESULTS

The CO 2-1 line were detected toward only six sources among the 58 observed in this survey. The baseline RMS noise of all observed data and the line parameters for the detected sources are given in Tables 1 and 2, respectively. A main beam efficiency of 0.75 is used to convert the antenna temperature  $T_A^*$  into main beam temperature  $T_{\text{mb}}$ . Also given in Table 2 are integrated line flux,  $F_{\text{int}}$ , and its ratio to the *IRAS* 25  $\mu\text{m}$  flux density

$$R_{\text{CO25}} = F_{\text{int}}/F_{25}. \quad (1)$$

<sup>2</sup>The Torun pAGB star catalogue is publicly available at: <http://www.ncac.torun.pl/postagb2>

Only good quality *IRAS* flux densities (with  $Q = 2$  or 3) are used in this work. The *IRAS*  $25\ \mu\text{m}$  flux density is considered because it is the representative wavelength of the cool dust emission from the circumstellar envelopes of all evolved stars considered here: AGB stars, pAGB stars, and PNe. In addition,  $25\ \mu\text{m}$  flux densities have smaller interstellar contamination than  $60\ \mu\text{m}$  flux densities for low galactic latitude objects which will be compiled from literature in the next section.

Among the six detected sources, there is only one new detection of CO 2-1 line in IRAS 07430+1115 (only its CO 1-0 line was detected before). The CO 2-1 line was observed but not detected toward this object by Hrivnak & Bieging (2005), which was perhaps due to the wrong source position used by them (the position they observed was away from the *IRAS* position by about  $30''$ , comparable to the beam size). The very narrow CO 2-1 line toward IRAS 19437-1104 is also new, but it is possibly a contamination from a high Galactic latitude molecular cloud, because: 1) so narrow CO line ( $V_{\text{exp}} = 0.7\ \text{km s}^{-1}$ ) is very rare among pAGB stars, and 2) the LSR velocity of the narrow CO line (at  $V_{\text{LSR}} = 3.58\ \text{km s}^{-1}$ ) is the same as an interstellar cloud toward the same direction as measured by Dame et al. (2001). Therefore, this object will not enter our discussions hereafter.

The resulting CO line profiles of the six detected sources are shown in Fig. 1. Here we give notes for some interesting spectral line features in these profiles.

1. A common feature of these CO 2-1 lines is the presence of high velocity line wings. Four of the five detected circumstellar CO lines show evidence of such line wings (with the only exception being IRAS 07430+1115, see Fig. 1). The Gaussian line wings are usually produced by fast (bipolar) winds from the central pAGB star.
2. The CO 2-1 line of IRAS 19500-1709 is a composite profile with a strong narrow feature superimposed at the center of a broader flat pedestal. Similar composite line profiles had been found in some other AGB or pAGB stars, such as RS Cnc (Gérard & Le Bertre 2003; Libert et al. 2010), EP Aquarii (Winters et al. 2007), and more such sources in Knapp et al. (1998) and Winters et al. (2003). The interpretation of such profile is still controversial, however.
3. The sharp peak CO line profile of IRAS 17534+2603 had been nicely interpreted by Bujarrabal et al. (2007) on the basis of their CO line interferometry data with a bipolar hourglass shaped outflow model.
4. A small narrow emission like feature can be recognized around  $V_{\text{LSR}} = 5\ \text{km s}^{-1}$  on the top of the broad line profile of Frosty Leo. A plateau was seen near the same velocity in a better quality line profile obtained with IRAM (with smaller beam) by Bujarrabal et al. (2001). The change of profile shape of this feature with different beam sizes indicates that it should originate from the circumstellar envelope instead of from interstellar clouds.
5. Absorption like features are present in the CO 2-1 line profile of two objects. An absorption like feature is seen in the blue line wing of IRAS 19500-1709 at  $V_{\text{LSR}} = 14.4\ \text{km s}^{-1}$ , or at a Doppler shift of  $\approx -10\ \text{km s}^{-1}$  with respect to the systemic velocity of  $24.4\ \text{km s}^{-1}$ . The same object was observed with IRAM 30m by Bujarrabal et al. (2001) and clearer absorption like features had been seen around similar velocities on top of broad line wings in their better profile data. As argued by Bujarrabal et al. (1992), it could be the signpost of still deeply embedded small-size fast winds. Similar absorption like features also appear in the blue line wing of IRAS 17436+5003 at Doppler shifts of -33, -23 and  $-14\ \text{km s}^{-1}$  with respect to the systemic velocity of  $-35.3\ \text{km s}^{-1}$  in Fig. 1. The bluest of the three absorption features even shows negative strength. Although the three absorption features in this object are weak, their appearance can be nicely confirmed in this object by comparing our data with previous observation of the same line with IRAM 30m telescope by Bujarrabal et al. (1992) more than 16 years ago. These absorption features were also briefly mentioned by Castro-Carrizo et al. (2004) with their more recent observations. Part of these weak

TABLE 1  
THE 58 OBSERVED HIGH GALACTIC LATITUDE POST-AGB STARS.

Name <sup>a</sup>	RA(2000) hh:mm:ss.sss	DEC(2000) dd:mm:ss.sss	RMS( $T_{\text{mb}}$ ) mK	Name <sup>a</sup>	RA(2000) hh:mm:ss.sss	DEC(2000) dd:mm:ss.sss	RMS( $T_{\text{mb}}$ ) mK
01005+7910	01:04:45.514	79:26:46.312	12	NGC 6254	16:57:11.743	-04:03:59.670	9
LX And	02:19:44.091	40:27:22.208	22	F17015+0503	17:04:00.085	04:59:00.816	8
05208-2035	05:22:59.424	-20:32:53.116	11	PG 1704+222	17:06:46.171	22:05:52.090	9
RV Col	05:35:44.206	-30:49:35.490	13	UZ Oph	17:21:59.260	06:54:42.217	10
06338+5333	06:37:52.422	53:31:02.017	9	V453 Oph	17:26:49.115	-02:23:36.146	12
07430+1115	07:45:51.390	11:08:19.626	8	17436+5003	17:44:55.470	50:02:39.465	14
09371+1212	09:39:53.963	11:58:52.604	13	F17495+0757	17:52:01.248	07:56:29.194	10
10158-2844	10:18:07.590	-28:59:30.840	22	17534+2603	17:55:25.182	26:02:59.964	16
DN Leo	10:38:55.230	10:03:48.500	18	18062+2410	18:08:20.083	24:10:43.323	11
11157+5257	11:18:33.583	52:40:54.606	8	18095+2704	18:11:30.670	27:05:15.547	15
11472-0800	11:49:48.040	-08:17:20.420	17	V443 Lyr	18:29:31.508	33:58:40.897	12
BD+13 2491	12:07:10.820	12:59:07.750	15	V534 Lyr	18:37:58.775	37:26:05.676	15
CD-31 9638	12:20:44.940	-32:33:26.190	20	19132-3336	19:16:32.759	-33:31:20.434	30
12538-2611	12:56:30.140	-26:27:36.950	19	F19179-3336	19:21:07.327	-31:23:50.323	22
BPS CS 22877-0023	13:25:39.470	-08:49:19.060	18	19437-1104	19:46:30.528	-10:56:54.934	13
13467-0141	13:49:17.120	-01:55:44.820	16	19500-1709	19:52:52.692	-17:01:50.358	22
F15160+0215	15:18:36.150	02:04:16.280	18	19590-1249	20:01:49.831	-12:41:17.779	14
F15240+1452	15:26:20.820	14:41:36.340	16	20023-1144	20:05:05.413	-11:35:57.915	13
BT Lib	15:31:15.890	-23:21:36.220	20	RX Cap	20:14:55.215	-12:56:34.702	25
15465+2818	15:48:34.407	28:09:24.264	13	V590 Aql	20:17:08.554	-04:03:06.991	22
BD+33 2642	15:51:59.882	32:56:54.373	15	FQ Aqr	20:51:21.341	02:18:46.360	18
BD+26 2763	15:58:58.275	26:08:04.646	15	20547+0247	20:57:16.284	02:58:44.554	30
LSE 29	16:09:24.560	-27:13:38.160	22	PHL 1580	21:30:25.244	-19:22:34.374	32
V2205 OPH	16:28:35.373	-09:19:31.814	20	NGC 7089	21:33:32.413	00:49:05.793	11
F16277-0724	16:30:30.020	-07:30:52.050	18	PHL 174	21:50:48.657	-19:42:00.270	20
NGC 6205	16:41:33.680	36:26:07.706	14	22006-1652	22:03:19.699	-16:37:35.245	34
V652 Her	16:48:04.693	13:15:42.282	16	22327-1731	22:35:27.528	-17:15:26.956	32
TT Oph	16:49:35.888	03:37:54.242	9	BD+39 4926	22:46:11.231	40:06:26.294	15
LS IV -04 1	16:56:27.731	-04:47:23.708	10	DS Aqr	22:53:17.037	-18:35:30.984	32

NOTE.—Positions and baseline RMS noise level of the observed CO 2-1 spectra.

<sup>a</sup>IRAS or FIRAS prefix has been omitted

TABLE 2  
CO LINE PARAMETERS OF THE SIX DETECTED HIGH GALACTIC LATITUDE POST-AGB STARS.

IRAS	Other Name	$l$ deg	$b$ deg	Sp.Type	$T_{\text{mb}}$ <sup>a</sup> mK	$V_{\text{exp}}$ <sup>a</sup> km s <sup>-1</sup>	$I_{\text{int}}$ <sup>a</sup> K.km s <sup>-1</sup>	$F_{\text{int}}$ <sup>a</sup> Jy MHz	$V_{\text{LSR}}$ km s <sup>-1</sup>	$R_{\text{CO25}}$ <sup>b</sup> MHz
07430+1115		208.9312	+17.0670	G5Ia	74(8)	6.5(0.6)	1.03(0.05)	35.0(1.7)	15.7	1.17(0.24)
09371+1212	Frosty Leo	221.8895	+42.7269	K7II	166(13)	22.8(0.8)	8.04(0.14)	273.7(4.8)	-15.6	59.62(11.97)
17436+5003	V814 Her	077.1331	+30.8696	F3Ib	256(14)	8.6(0.4)	4.71(0.10)	160.3(3.4)	-35.3	0.87(0.18)
17534+2603	89 Her	051.4341	+23.1876	F2Ibe	233(16)	3.5(0.3)	1.75(0.07)	59.6(2.4)	-8.4	1.09(0.22)
19437-1104	DY Aql	029.1826	-17.1308	G5	122(13)	0.7(1.3)	0.17(0.03)		3.6	
19500-1709	V5112 Sgr	023.9837	-21.0361	F2/ F3Iab	259(22)	10.4(1.2)	5.77(0.24)	196.4(8.2)	24.4	1.19(0.24)

<sup>a</sup>The values in the parentheses are  $1\sigma$  noise level.

<sup>b</sup> $R_{\text{CO25}}$  is defined by Eq. 1 in Sect. 3.

but stable absorption features could be similarly interpreted by embedded small-size fast winds, as for the case of IRAS 19500-1709. The absorption with negative flux could also be interpreted similarly given that continuum emission is strong enough in the compact outflow regions. However, it is hard for this scenario to explain all the three absorption features in this line profile with simple CSE structures. Similar absorption line features have been found in the CO line profiles of other well-known AGB or pAGB stars, e.g., CRL 2688 (Kawabe et al. 1987; Cox et al. 2000; Bujarrabal et al. 2001), CRL 618 (Hajian et al. 1996; Sánchez Contreras et al. 2004), and some other sources from Castro-Carrizo et al. (2010).

#### 4. LITERATURE DATA

Because the detection rate of CO 2-1 line in our high Galactic latitude pAGB star sample turns out to be low, we complement our sample with compilation of literature CO 2-1 line data for all 393 known pAGB stars (including likely, RCrB-eHe-LTP and RV Tau types) from the second version of the Torun Catalog (Szczerba et al. 2012). Here eHe means extreme helium stars, while LTP stands for Late Thermal Pulse objects. The details of the data compilation are given in Appendix A. Only the summary of the literature data are given here.

In total, the compilation by October 26, 2011 includes 175 literature CO 2-1 line data entries (see Tables 5 and 6 in Appendix A) of 87 pAGB stars. The repeated observations have been averaged together to yield the most representative CO 2-1 line flux for each of these 87 objects. They are presented in Table 7 in Appendix A, together with IRAS flux densities, IRAS colors and the ratio between integrated CO 2-1 line flux and IRAS  $25\ \mu\text{m}$  flux density.

After combining this with our high Galactic latitude sample and removing duplicated objects, the total number of observed pAGB stars is 133, among which 44 objects were detected in CO 2-1 line. Thus, about 34 per cent of the known pAGB stars have been observed in the CO 2-1 line, and the detection rate is also about 34 per cent.

According to the analysis of the statistical prop-

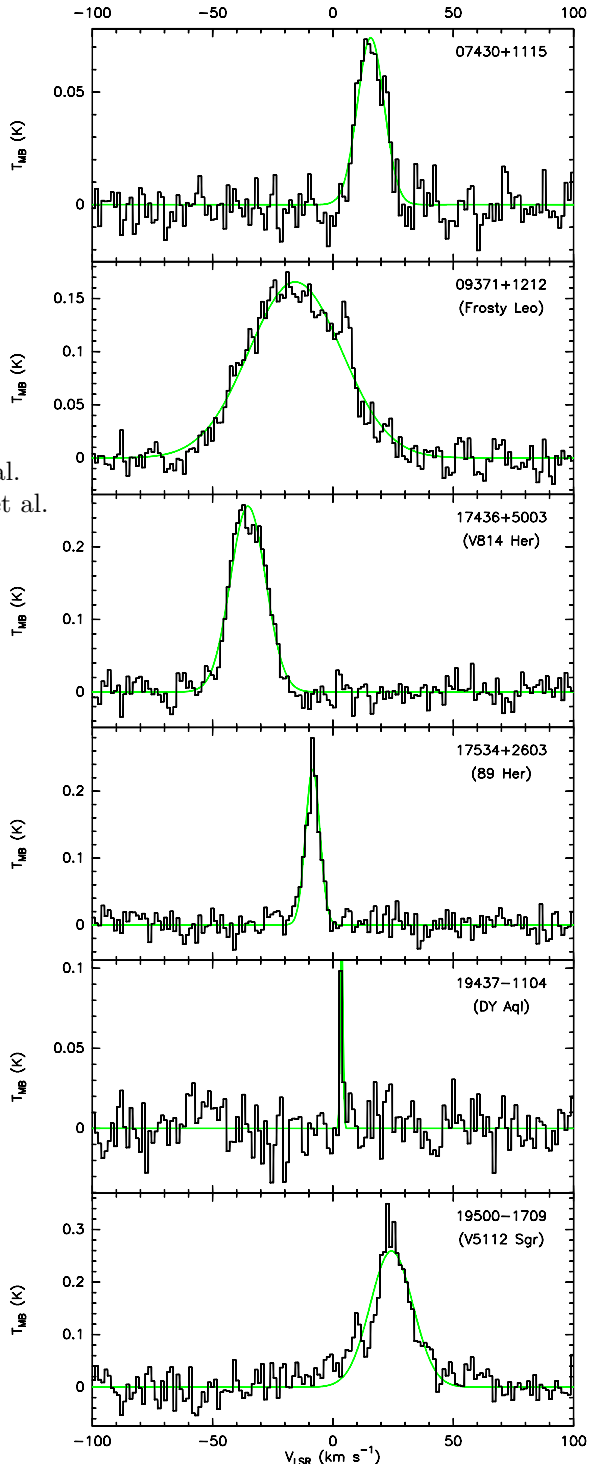


Fig. 1.— The observed CO 2-1 line spectra of the detected high Galactic latitude post-AGB sample stars. Overplotted smooth curves are Gaussian fittings. The very narrow line of IRAS 19437-1104 is possibly a contamination from an interstellar cloud (see details in Sect. 3).

erties of the observed sample (see Appendix B), it is found that the available CO 2-1 observations have the following bias effects: 1) pAGB stars in the Galactic Center direction are under-represented; 2) the available CO 2-1 line observations are biased to strong IR emitters and the detectability of CO 2-1 line is sensitivity limited.

In addition, 1117 CO 2-1 line data entries are collected for 751 other objects (AGB stars and PNe) from the following papers for the purpose of comparison with pAGB stars: the compilation of Loup et al. (1993); some S stars from Jorissen & Knapp (1998); Ramstedt et al. (2009); some PNe from Huggins et al. (2005, 1996); and some O-rich semiregular and irregular variables from Kerschbaum & Olofsson (1999). Among them are 569 AGB stars (28 OH/IR stars plus another 155 O-rich AGB stars, 56 S stars, and 330 C-rich AGB stars) and 182 PNe. Repeated CO observations for these objects are also averaged together, as it was done for pAGB objects. We do not present the detailed data in this paper, however, since they are not complete compilations for any of these type of objects.

The IRAS point source flux densities of these objects are also extracted from the IRAS Point Source Catalog and in a few cases from the IRAS Faint Source Catalog. Only those good quality IRAS data (with the quality factor  $Q > 1$ ) are used in this work.

## 5. DATA ANALYSIS

### 5.1. CO-IR relation of high and low Galactic latitude post-AGB stars

Although the relation between CO line strength and infrared dust emission strength has been studied before (e.g., Bujarrabal et al. 1992), it is still lack of in-depth investigation. In this work, we do not try to compare the dust and gas mass loss rates. Instead, we directly compare the observed CO line fluxes with *IRAS* flux densities ( $R_{\text{CO25}}$  ratio - see Eq. 1). The greatest advantage of the direct comparison is that it allows to exclude the uncertainties introduced by distances and empirical formulas for mass loss rate. The traditional *IRAS* color-color (C-C) diagram of the two colors,

$$\begin{aligned} \text{C12} &= 2.5 \log(F_{25\mu\text{m}}/F_{12\mu\text{m}}), \\ \text{C23} &= 2.5 \log(F_{60\mu\text{m}}/F_{25\mu\text{m}}), \end{aligned}$$

is also used. Here,  $F_{12}$ ,  $F_{25}$  and  $F_{60}$  are the IRAS flux densities. The C23 color is a better tracer of the cool dust emission around pAGB stars than C12. Thus, we will concentrate on  $R_{\text{CO25}}$ -C23 relationships of our sample stars.

Our new observational results of the high Galactic latitude (h.g.l.) pAGB stars are combined with literature data. The h.g.l. objects (we adopt  $|b| > 15^\circ$ ) should be mainly local stars or low mass halo stars statistically less massive than the low Galactic latitude (l.g.l.) counterparts. Thus, we plot their  $R_{\text{CO25}}$ -C23 and IRAS C-C diagrams separately in Fig. 2. Compared with our new observations, there is no CO 2-1 line detections in literature toward other h.g.l. objects. However, the average literature CO line fluxes show clear discrepancies with our new measurements for Frosty Leo and 89 Her (see the two symbols linked to the same object names in the figure). The lower literature CO line flux of 89 Her could be due to the fact that it has been partially resolved by the small beam of the IRAM telescope which was used to obtain two of the three available literature CO datasets. For Frosty Leo, the literature data was obtained by a 12m telescope (similar as in this work) more than 18 years ago. The reason for the discrepancy is unclear. The  $1-\sigma$  upper limits of non-detection sources are estimated by assuming a typical CSE expansion velocity of  $10 \text{ km s}^{-1}$  ( $\approx 7.7 \text{ MHz}$ ). The  $R_{\text{CO25}}$ -C23 diagram will be called CO-IR diagram hereafter.

Shown in the upper panels of Fig. 2 are h.g.l. pAGB stars. Both the literature data (gray circles) and our new observations (black dots for the detected objects) are shown, as indicated by double arrows in the figure. In the upper left panel, almost all the detected pAGB stars, excluding the only exceptional case of Frosty Leo, show very similar CO-IR flux ratios of

$$R_{\text{CO25}} \approx 1.04(\pm 0.08)[\text{MHz}] \quad (2)$$

as delineated by the horizontal line in the figure. This relation is valid in the color range of  $-1.6 < \text{C23} < 0.0$  for the considered pAGB stars. The slant dashed line will be explained below.

On the IRAS C-C diagram in the upper right panel, Frosty Leo is not shown because of the poor quality of its *IRAS*  $12\mu\text{m}$  flux density data. The remaining four objects are distributed along an elongated region below the black body line. Par-

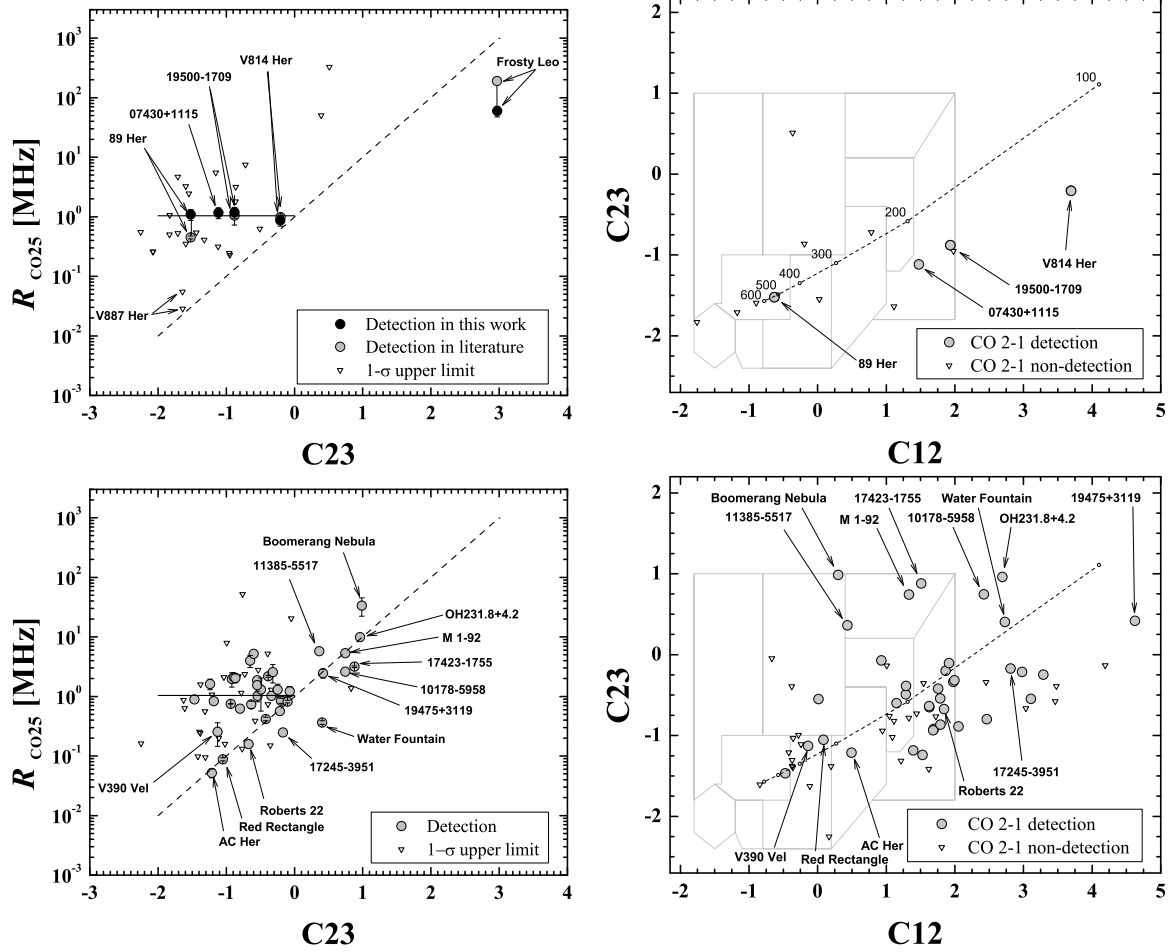


Fig. 2.— The integrated CO 2-1 line flux to *IRAS* 25  $\mu\text{m}$  flux density ratios ( $R_{\text{CO}25}$  - see Eq. 1 in Sect. 3) are plotted against *IRAS* color C23 (the so called CO-IR diagram defined in Sect. 5.1) for the observed high and low Galactic latitude pAGB stars in the left top and bottom panels, respectively. Also shown, in the right panels, are the traditional *IRAS* color-color diagrams for the same groups of pAGB objects. The error bars are the 20 per cent nominal uncertainty of the CO line fluxes. The horizontal solid line and slant dashed line on the CO-IR diagrams represent the major trends of the pAGB star distribution. The short dashed line on the *IRAS* C-C diagrams is the black body (BB) line with integer numbers being the BB temperatures. The regions in the *IRAS* C-C are those defined by van der Veen et al. (1989) for evolved stars.

ticularly, the C12 colors vary more than the C23 colors. This trend of increasing colors could be the result of fast weakening of the  $12\mu\text{m}$  flux density when the inner CSE of the pAGB stars is gradually evacuated. Thus, the increasing IR color sequence of the detected h.g.l. pAGB stars could be an evolutionary sequence. Two special objects are commented in the footnote<sup>3 4</sup>.

In the two lower panels of Fig. 2, the l.g.l. pAGB stars are shown. The CO-IR diagram in the lower left panel shows that many stars with CO detection (gray circles) are crowded around a similar region as the high latitude stars (with  $R_{\text{CO}25} \approx 1.04$  and  $\text{C}23 < 0.0$ ), while the rest objects seem to be located in an elongated region, extending from blue C23 color and small  $R_{\text{CO}25}$  ratio to red C23 color and large  $R_{\text{CO}25}$  ratio. The object names are marked out in the figure for the latter group of stars. We find that a slant straight line (the dashed line) of

$$\log(R_{\text{CO}25}) \approx \text{C}23. \quad (3)$$

can represent this trend reasonably well. This log-linear trend holds in the color range of  $-1.2 < \text{C}23 < 1$ . Eq. 3 is not a fit to the data, but a simple function recognized by eyes. The lower right corner of this CO-IR diagram is devoid of objects, hinting that this log-linear trend could represent a border of pAGB star distribution on the CO-IR diagram.

The l.g.l. pAGB objects, which are distributed along the slant line and have  $\text{C}23 < 0$  are located on or below BB line on the IRAS C-C diagram. On the other hand, the rest objects that have

<sup>3</sup> Frosty Leo stands out with its very red C23 color and very high  $R_{\text{CO}25} \approx 60$  in the upper left panel of Fig. 2. Although the very red C23 color can be partially attributed to its very strong water ice emission band around  $46\mu\text{m}$  (Forveille et al. 1987), the very large  $R_{\text{CO}25}$  ratio needs other mechanisms or explanation. This object also has other peculiar properties such as a high initial stellar mass of  $4.23 M_{\odot}$  (Murakawa et al. 2008), a massive compact expanding ring seen in CO 2-1 and 1-0 lines and in near-IR polaro-imaging data (Castro-Carrizo et al. 2005; Dougados et al. 1990) around a binary system (Roddiier et al. 1995), and frenzied equatorial jets (Sahai et al. 2000).

<sup>4</sup> V887 Her is also peculiar in that the  $1\text{-}\sigma$  upper limit of the  $R_{\text{CO}25}$  ratio is more than 10 times smaller than that of the five CO detections in the upper left panel of Fig. 2. It is an RV Tauri variable (Şahin et al. 2011) showing depletion of refractory elements such as Al, Y and Zr.

$\text{C}23 > 0$  (with the exception of IRAS 19475+3119) are located above BB line (see the lower panels of Fig. 2). In addition, it is seen that the l.g.l. pAGB stars, which appear in a similar region as the h.g.l. ones on the CO-IR diagram (compare the two left panels) also occupy a similar region on the IRAS C-C diagrams (compare the two right panels). This indicates that these h.g.l. and l.g.l. objects share a similar combination of dust and CO gas characteristics.

## 5.2. CO-IR diagrams in the context of AGB-pAGB-PN sequence

Although some regularity has begun to emerge on the previously discussed  $R_{\text{CO}25}$ -C23 diagrams of the pAGB stars, the discussed trends are still murky due to the limited number of objects involved. In this section, we try to verify these trends in a broader context of the AGB-pAGB-PN evolutionary sequence. The CO 2-1 line data collected from literature for some AGB stars and PNe make this comparison possible. Thus, the CO-IR diagrams of these AGB stars and PNe are plotted and compared with the pAGB stars (represented by the two straight lines that delineate the major trends) in Fig. 3. The traditional IRAS C-C diagrams are also shown for them. For clarity, the C-rich and O-rich AGB stars are plotted in separate panels.

### 5.2.1. AGB stars and PNe on the CO-IR diagrams

We briefly discuss the distribution of AGB stars and PNe on the CO-IR and IRAS C-C diagrams, while more comparison among these objects is presented in Appendix C.

In the top left panel of Fig. 3, C-rich AGB stars (empty circles) mainly concentrate in a compact region on the  $R_{\text{CO}25}$ -C23 diagram, and S stars (gray filled circles) mainly scatter in a similar region as the C stars. On the IRAS C-C diagram (the top right panel), most of these stars are distributed slightly below the black body line (the dotted line) or in regions with red C23 but blue C12 colors. Their mean IR color is  $\text{C}23 = -1.54 \pm 0.35$  and their mean CO-IR flux ratio is  $\log(R_{\text{CO}25}) = 0.41 \pm 0.40$ .

In the middle left panel of Fig. 3, many O-rich AGB stars (empty circles) concentrate in another



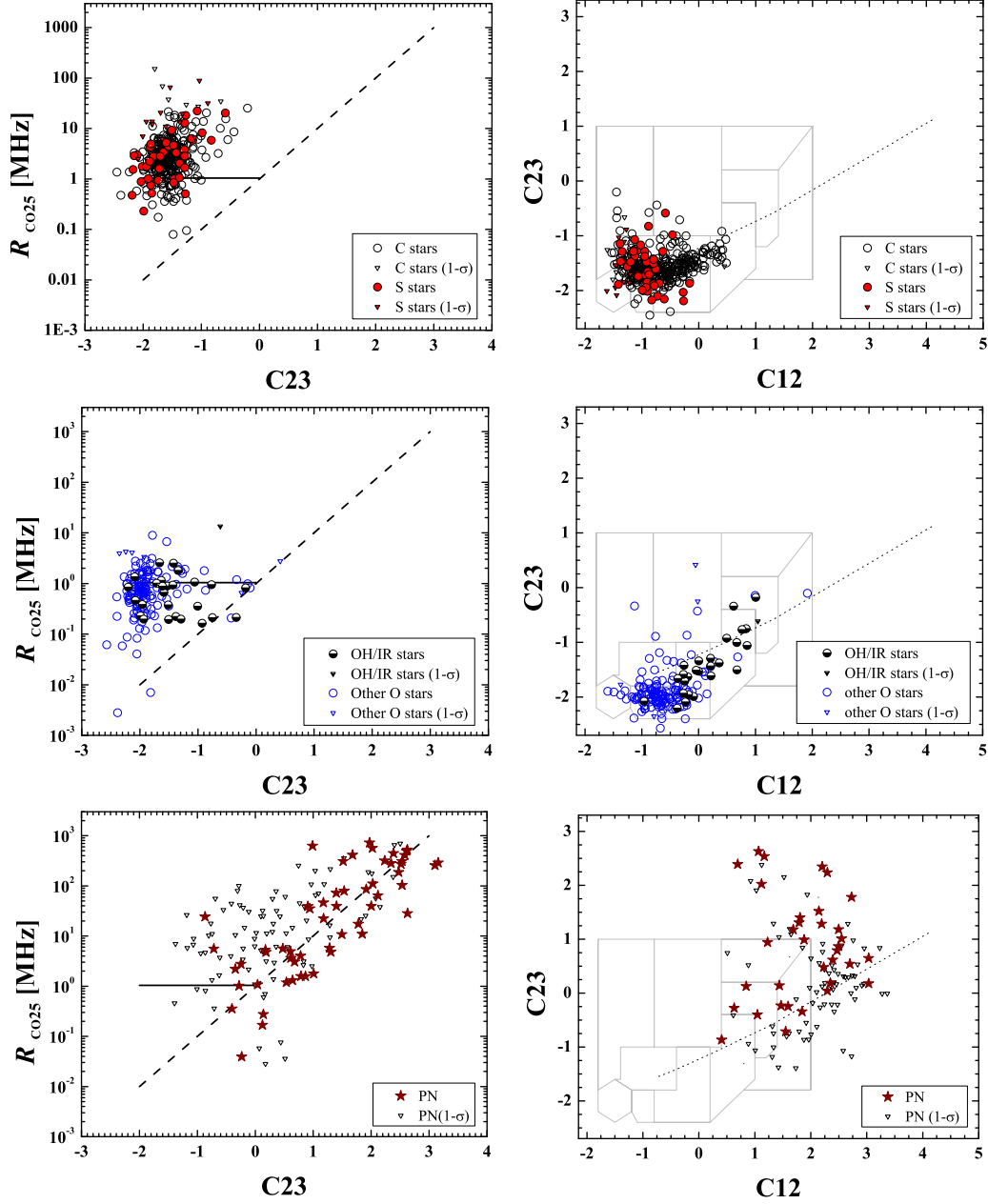


Fig. 3.— The same as Fig. 2 but for C- and O-rich AGB stars and PNe. The trends of pAGB stars distribution are represented by the two lines on the CO-IR diagrams. A color plot is provided in the online version.

compact region different from that of C stars on the CO-IR diagram, whilst an extreme subsample of them — OH/IR stars (half-shaded black circles) — scatter in regions with similar or smaller  $R_{\text{CO}25}$  ratios but usually redder C23 colors than the other O-rich AGB stars. Their mean IR color is  $\text{C}23 = -1.70 \pm 0.76$  and their mean CO-IR flux ratio is  $\log(R_{\text{CO}25}) = -0.13 \pm 0.58$ , which means that they are slightly bluer and have 3.5 times smaller mean  $R_{\text{CO}25}$  ratios than C-rich AGB stars on average. On the IRAS C-C diagram in the middle right panel of the figure, most of these O-rich AGB stars concentrate in a region below the black body line, while the OH/IR stars stretch out to much redder regions, as expected.

In the bottom left panel of Fig. 3, PNe show a pronounced increasing log-linear trend on the CO-IR diagram. The trend spans more than 4 orders of magnitude of the  $R_{\text{CO}25}$  ratio and are in close agreement to the log-linear trend of pAGB stars (the dashed line). On the IRAS C-C diagram in the bottom right panel, most of the PNe appear in a very red region above the black body line, as expected for cold dusty CSEs.

### 5.2.2. The pAGB trends on the CO-IR diagram in the context of AGB-pAGB-PN evolution

By comparing the pAGB stars (represented by the two straight lines) with AGB stars and PNe in Fig. 3, it is now clear that the pAGB stars are distributed in a transitional region between the AGB stars and PNe on the CO-IR diagram. The subgroup of pAGB stars represented by the horizontal solid line in the figure have similar CO-IR ratios (with a mean  $\log(R_{\text{CO}25}) = 0.02 \pm 0.03$ ) as AGB stars, but have redder IR colors (with  $\text{C}23 = -1.6 \sim 0.0$ ). The log-linear trend followed by the rest group of pAGB stars on the CO-IR diagram agree quite well with the trend of PNe. Thus those pAGB stars with very red C23 colors ( $> 0$ ) could be the precursor of the shown PNe. The other end of the log-linear trend (with  $\text{C}23 < 0$ ) is populated by some pAGB stars that have exceptionally small  $R_{\text{CO}25}$  (very weak CO line emission).

The distinctive characteristics of these pAGB stars allow us to divide them into three subgroups, which, as we show later, have different properties.

### 5.3. Grouping of post-AGB stars

Our sample of pAGB stars aggregate in different regions on the CO-IR diagram, which is not so well seen on the traditional IRAS C-C diagram. As we will see below, the aggregation on the CO-IR diagram just reflects different nature (e.g., mass, binarity, chemistry, etc.), and the stage of pAGB evolution of these stars through the contrast of dust and CO line emission. Here, we merge the h.g.l. and l.g.l. pAGB stars and divide them into three CO-IR groups, as shown in the upper panel of Fig. 4. Only significant, from point of view of performed source classification, CO non-detections are plotted in Fig. 4.

*group-I* — those pAGB stars with  $R_{\text{CO}25} > 1/3$  and  $\text{C}23 < 0$  (the red filled circles, or gray filled squares in Fig. 4). They compose the largest group of pAGB stars, which is distributed in a horizontally elongated region on the CO-IR diagram, with similar  $R_{\text{CO}25}$  ratio of  $\sim 1$  MHz (actually in the range of 0.42-5.2 MHz, with a median of  $\sim 1$  MHz). Their distribution can be roughly represented by the horizontal line that was determined for our h.g.l. pAGB stars in Sect. 5.1.

*group-II* — those pAGB stars with  $\text{C}23 > 0$  (the green filled circles and one gray filled square in Fig. 4). They are the reddest group with usually enhanced CO 2-1 emission relative to their IR dust emission. They occupy the red part of the log-linear trend as delineated by the dashed line in the figure.

*group-III* — those pAGB stars with  $R_{\text{CO}25} < 1/3$  and  $\text{C}23 < 0$  (the blue filled circles in Fig. 4). They have exceptionally weak CO 2-1 line emission, although their C23 colors are similar to that of group-I stars. They occupy the blue part of the log-linear trend (the dashed line) and the region immediately above it. This group also includes some CO 2-1 non-detections whose  $1-\sigma$  upper limit of  $R_{\text{CO}25}$  ratios are smaller than  $1/3$  and thus they are also CO deficient pAGB stars. We did not plot the other non-detections, since they could be members of different groups.

All of the three CO-IR groups of pAGB stars are listed in Table 3, with different groups in separate sub-sections of the table. The vicinity of intersection between the solid and dashed lines in the top panel of Fig. 4 do not allow us to be sure to which group a given object belong. Therefore, the

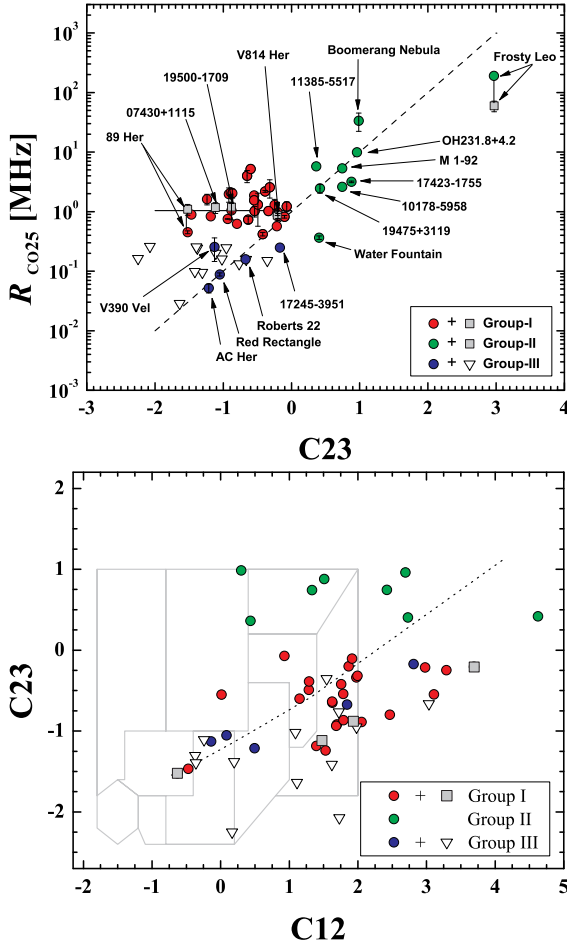


Fig. 4.— Grouping of all pAGB stars on the CO-IR diagram and the resulting groups on the *IRAS* C-C diagram. The lines and regions are the same as in Fig. 2. Object names are labelled out for our five high Galactic latitude pAGB stars and the CO-detected pAGB stars that belong to groups-II and III.

classification of the objects near the group borders (here we have assumed somewhat arbitrarily a rectangular border region as  $R_{\text{CO}25} > 1/3$  and  $-0.5 < \text{C}23 < 0$ ) is tentative, and we labeled them with a leading ‘\*’ symbol before their object names in Table 3. The table is organized in a way to enable easy comparison between the CO-IR and IRAS C-C diagrams in Fig. 4. Objects in groups-I and II are sorted with the increasing C23 colors, while those of group-III are ordered in decreasing C23 colors. Also listed in the table are some properties of the pAGB stars that will be explained and discussed later in Sect. 6.

In the lower panel of Fig. 4, the three groups are displayed also on the traditional dust emission diagnostic tool, the IRAS C-C diagram. Group-II pAGB stars are clearly separated from the other stars by their large C23 colors. However, the groups-I and III pAGB stars are well mixed on the IRAS C-C diagram, which demonstrates that the involvement of gas emission (the CO 2-1 line) in the grouping does have brought us a new information about the pAGB stars.

Group-I pAGB stars distribute in an elongated region on the IRAS C-C diagram, with their C23 colors varying only by a factor about 1.5, while their C12 colors varying by a larger factor of about 4.0. The larger variation range of the C12 colors may be the natural consequence of fast weakening of the  $12\mu\text{m}$  dust emission in the expanding detached CSE. Thus, group-I pAGB stars are possibly still in early pAGB stage when the detached CSE is still actively developing, which is also supported by the fact that their  $R_{\text{CO}25}$  ratios are similar to that of AGB stars. Their similar  $R_{\text{CO}25}$  ratios hints that the thermal balance in the gas (represented by the CO 2-1 line) and dust (represented by the  $25\mu\text{m}$  emission) could be still tightly coupled during the early pAGB stage.

The red C23 color and richness of CO 2-1 emission of the group-II stars indicate that they could have massive and cool CSEs. To the opposite, the weakness of CO 2-1 emission and the blue C23 colors of the group-III stars suggest that they could be lower mass pAGB stars with more transparent spherical component in their CSEs where CO molecules have been partially or totally destroyed by penetrating UV photons. The well known low mass binary disc system Red Rectangle (Men’shchikov et al. 2002;

Witt et al. 2009) that shows narrow CO line (Jura et al. 1995; Dayal & Bieging 1996) is just a member of the group-III. However, it is not clear why the distinct groups-II and III share the same log-linear relationship on the CO-IR diagram.

## 6. DISCUSSION

As we showed in Sect. 5, the AGB, pAGB and PN CO-emitters segregate into different regions on the CO-IR diagram, which sets up a new platform for discussing the various aspects of the pAGB stars evolution. In this section, we consider chemical and central star spectral types, spectral energy distribution (SED) types, binarity, CSE expansion velocities of the pAGB stars, and their pAGB sub-types to investigate evolution and diversity of these objects using CO-IR diagram.

To facilitate the discussion, we collect the important properties of the three groups of pAGB stars in Table 3. Altogether, excluding 32 non-detections with upper limit of  $R_{\text{CO25}} > 1/3$ , we have gathered information for 55 objects. There are following columns in the table: Object name, C23 - IRAS color,  $R_{\text{CO25}}$  - CO to IR flux ratio,  $V_{\text{exp}}$  - CSE expansion velocity, SED - spectral energy distribution type, Binarity, Chem.type (\* / CSE) - central star and CSE chemical type, Spectral type - central star spectral type, pAGB class, and Chem.ref (\* / CSE) - literature for chemical type of the star and CSE. The references for chemical and spectral types are given in footnotes to Table 3. Most of the data are already collected in the Torun Catalog, but not yet for chemistry of central stars and their circumstellar envelopes. Therefore, we have performed dedicated literature study to determine chemical types (but also to fine-tune spectral types) of pAGB objects, so credits to the original works or compilations are given below Table 3. Note that chemistry of CSE is also inferred from dust features seen in Infrared Space Observatory (ISO) spectra (if available in several cases) which can be found in the Torun catalog.

### 6.1. Chemical and spectral types of post-AGB objects

For discussion in this paper, we assume that the chemical type of a pAGB object is C-rich if it has a C-rich central star and/or C-rich dust in its CSE. Also stars with dual dust chemistry in their

CSE (simultaneous presence of C- and O-rich dust features and/or molecules) are treated as having C-rich chemical type. Knowledge of chemical type is important since it allows to roughly estimate mass of the progenitor. Single carbon stars are formed only in a limited progenitor mass range. For solar metallicity this happens for  $\sim 1.5 M_{\odot} < M_{\text{ZAMS}} < \sim 5 M_{\odot}$ , and the mass range shrinks and shifts towards somewhat smaller values for lower metallicities (Piovan et al. 2003). For progenitor mass lower and higher than the above mass range a star will remain O-rich. Note, however, that in close binary systems, mass transfer to a companion star may reduce the star's AGB lifetime and the star may remain O-rich even if its progenitor was of intermediate mass.

The distribution of the chemical types from Table 3 is visualized together with central star spectral types on the CO-IR diagram in Fig. 5. C-rich and O-rich pAGB stars are plotted in separate rows, while those with late and early spectral types in different columns.

In the left two panels of Fig. 5, the C- and O-rich pAGB stars with late spectral types (F, G, K and M) show distinctive distributions. C-rich pAGB stars of late spectral types are mostly group-I sources, with only few objects, like Red Rectangle, Roberts 22 and IRAS 19477+2401<sup>5</sup>, belonging to group-III. On the other hand, O-rich pAGB stars with similar spectral types belong predominantly to group-III<sup>6</sup>, and to the transition region between different groups. Group-II objects with late spectral types are not numerous, in general, but among them there is only one C-rich star (IRAS 11385-5517) with SiC emission at  $11.3 \mu\text{m}$  seen in its ISO spectrum, but also with OH emission detected from its shell (see Torun catalog and references in Table 3).

Post-AGB stars of earlier spectral types (right panels of Fig. 5) are also not numerous in our sample but are located mostly along the log-linear track (dashed line in the figure), with a clear exception being V886 Her (C23 = -2.07) - a massive (Ryans et al. 2003) fast evolving O-rich pAGB star (Arhipova et al. 1999).

<sup>5</sup>This object shows the '21 micron' feature, but its  $R_{\text{CO25}}$  is uncertain due to interstellar contamination of the CO 2-1 emission (Hrivnak & Bieging 2005).

<sup>6</sup>As we show in the next subsection this group contains a significant number of known binary systems.

TABLE 3  
 PROPERTIES OF THE THREE CO-IR GROUPS OF POST-AGB STARS.

Object name	C23	RCO25	$V_{\text{exp}}$ km s <sup>-1</sup>	SED <sup>a</sup>	Binar <sup>a</sup>	Chem. type */CSE	Spectral <sup>s</sup> type	pAGB <sup>a</sup> class	Chem.ref <sup>c</sup> */CSE
----- Group I -----									
89 Her	-1.52	1.09 <sup>b</sup>	3.5 <sup>b</sup>	0	B	O/O	F2Ibe	UU Her	24/10
Al Sco	-1.47	0.89	2.8	0	B	C?/O	G4	RV Tau	9/8
22272+5435	-1.24	1.62	10.1	IVa		C/C	G5Ia	21 micron	1
04296+3429	-1.18	0.83	12.8	IVa		C/C	F3I <sup>(s1)</sup>	21 micron	1
07430+1115	-1.12	1.17 <sup>b</sup>	6.5 <sup>b</sup>	IVa		C/C	G5Ia	21 micron	1
20000+3239	-0.94	0.75	12.2	IVa		C/C	G8Ia	21 micron	1
07134+1005	-0.92	1.97	9.9	IVb		C/C	F7Ie <sup>(s2)</sup>	21 micron	1
16594-4656	-0.89	2.10	14.0	III		C/C	Ae <sup>(s2)</sup>	21 micron	1
19500-1709	-0.88	1.19 <sup>b</sup>	10.4 <sup>b</sup>	IVb		C/C	F0Ie <sup>(s2)</sup>	21 micron	1
23304+6147	-0.87	2.04	12.1	IVa		C/C	F6I <sup>(s3)</sup>	21 micron	1
14488-5405	-0.80	0.62	15.0	IVb		?/?	A0Ie <sup>(s2)</sup>	possible	-/-
06530-0213	-0.65	3.99	11.3	IVa		C/C	G1I <sup>(s2)</sup>	21 micron	1
17441-2411	-0.63	0.73	12.5	III		?/?	F4I <sup>(s2)</sup>	IRASsel	-/-
08005-2356	-0.60	5.20	100.0	I		C/O	F5Ie <sup>(s2)</sup>	IRASsel	2/15
23541+7031	-0.55	1.55	54.0	II		?/O	Be	hotpAGB	-/29
22223+4327	-0.55	1.87	14.0	IVb		C/C	F7I <sup>(s2)</sup>	21 micron	1
19454+2920	-0.54	1.02	15.6	III		?/C		IRASsel	-/11
* 19480+2504	-0.49	1.31	17.5	III		C/C		IRASsel	7/19
* 20028+3910	-0.42	0.42	14.5	III		?/O	F3-7I <sup>(s1)</sup>	IRASsel	-/10
* 22574+6609	-0.39	2.18	19.8	II		C/C		21 micron	1
* 09032-3953	-0.34	1.02	25.0	II		?/?		IRASsel	-/-
* 23321+6545	-0.32	2.56	16.1	III		?/C		IRASsel	-/11
* 19114+0002	-0.25	1.29	31.5	IVa		O/O	F7I <sup>(s2)</sup>	IRexc	24/15
* 17106-3046	-0.21	0.57	1.0	III		?/O	F5I <sup>(s2)</sup>	IRASsel	-/28
* V814 Her	-0.21	0.87 <sup>b</sup>	8.6 <sup>b</sup>	IVb		O/O	A7I <sup>(s2)</sup>	UU Her	24/15
* 17150-3224	-0.20	0.85	14.8	III		?/O	F3-7I <sup>(s1)</sup>	OHmaser	-/12
* 18276-1431	-0.10	0.82	12.2	IVa		?/O	K2/K3:II/III:	OHmaser	-/30
* CRL 618	-0.07	1.22	16.7	II		C/C	B0	refneb	4
----- Group II -----									
11385-5517	0.36	5.74	45.0	0	B	C/O	F0Iape	IRexc	24/31
Water Fountain	0.41	0.37	46.0	II		?/O		Water fountain	-/14
19475+3119	0.42	2.45	15.1	IVb		O/O	F3Ib	IRASsel	24/32
M 1-92	0.74	5.34	32.5	III	B	?/O	B0.5IV;F2	refneb	-/26
10178-5958	0.75	2.61	13.0	III		?/C	BIe <sup>(s2)</sup>	hotpAGB	-/20
17423-1755	0.88	3.17	26.5	II/III	B	?/O	Be	IRASsel	-/17
OH 231.8+4.2	0.96	9.94	21.4	II/III		O/O	M6	possible	16/18
Boomerang Neb	0.99	33.60	25.5	II		?/?		refneb	-/-
Frosty Leo	2.97	59.62 <sup>b</sup>	22.8 <sup>b</sup>	IVb	B	?/O	K7II	hgls	-/32
----- Group III -----									
17245-3951	-0.17	0.25	15.0	III		?/O	F6I <sup>(s2)</sup>	OHmaser	-/27
19374+2359	-0.35	< 0.15		II		?/O	B3-6I	IRASsel	-/13
19306+1407	-0.66	< 0.16		IVa		?/C,O	B0-1I <sup>(s1)</sup>	IRASsel	-/10
Roberts 22	-0.67	0.16	31.0	II		?/C,O	A0Ie <sup>(s2)</sup>	OHmaser	-/10
19477+2401	-0.77	< 0.13		II		C/C	G0I <sup>(s1)</sup>	21 micron	1
01005+7910	-0.95	< 0.25		IVb		?/C	B2Iab:e	hgIBsg	-/5
19386+0155	-1.02	< 0.16		I		O/O	F5I <sup>(s2)</sup>	IRASsel	22
Red Rectangle	-1.05	0.09	4.9	II	B	C/C,O	B8V	refneb	2/3,21
RV Tau	-1.11	< 0.20	0	0	B	C/?	K3pvar	RV Tau	24/-
V390 Vel	-1.13	0.25	5.6	I	B	O/?	F3e	RV Tau	24/-
AC Her	-1.21	0.05	1.5	0	B	O/O	F4Ibpvar	RV Tau	24/10
U Mon	-1.30	< 0.09	0	0	B	O/?	K0Ibpvar	RV Tau	24/-
DY Ori	-1.38	< 0.24	0	0	B	O/O		RV Tau	24/8
AR Pup	-1.39	< 0.25		III	B	O/?	F0Iab:...	RV Tau	24/-
Al CMi	-1.41	< 0.10		I		O/O	K3/5I <sup>(s2)</sup>	RV Tau	23/19
V887 Her	-1.64	< 0.03		IVa		O/O	F3Ib	OHmaser	25/6
V886 Her	-2.07	< 0.26		IVb		O/O	B3e <sup>(s2)</sup>	IRASsel	24/5
20004+2955	-2.25	< 0.16		0		?/O	G7Ia	IRexc	-/33

NOTE.—\* These objects appear near the joint region between the three CO-IR groups and thus their group identities are tentative. (Objects are sorted by C23 color within each group.)

<sup>a</sup>SED types, binarity and the sub-types of post-AGB stars are taken from the Torun Catalog.

<sup>b</sup>These values are preferentially taken from this work, instead of from literature.

<sup>c</sup>The circumstellar/central star chemical types were originally compiled from the CO data papers and SIMBAD database, but are later refined with dedicated literature study. Here is the list of the dedicated references and relevant comments: 1) Carbon rich star with 21 *micron* dust feature; 2) Bakker et al. (1997) (optical spectrum); 3) Waters et al. (1998) (ISO spectrum); 4) Stephenson (1989); 5) Cerrigone et al. (2009) (Spitzer: PAH/Silicates); 6) Eder et al. (1988) (OH maser); 7) Alksnis et al. (2001); 8) Gielen et al. (2011) (Spitzer: Silicate); 9) Giridhar et al. (2005) (optical spectrum); 10) Hodge et al. (2004) (ISO spectrum); 11) Hony et al. (2002) (30  $\mu$ m feature); 12) Hu et al. (1993) (OH maser); 13) Kwok et al. (1987) (CFHT IR photometry); 14) Likkell & Morris (1988) (OH & H<sub>2</sub>O masers); 15) Likkell (1989) (OH maser); 16) Spectral type of M6 in Simbad; 17) Manteiga et al. (2011) (Spitzer: Silicate & H<sub>2</sub>O ice absorption); 18) Morris & Bowers (1980) (OH maser); 19) Omont et al. (1993) (IR + HCN/CO); 20) Parthasarathy et al. (2001) (ISO: PAH); 21) Peeters et al. (2002) (ISO: PAH); 22) Pereira et al. (2004) (Optical and IR spectra); 23) Rao et al. (2012) (Spitzer: Silicate & H<sub>2</sub>O ice absorption); 24) Stasińska et al. (2006) (abundance compilation); 25) Şahin et al. (2011) (optical spectrum); 26) Seaquist et al. (1991) (OH maser); 27) Sevenster (2002) (OH maser); 28) Silva et al. (1993) (OH maser); 29) Volk & Kwok (1987) (IRAS/LRS); 30) te Lintel Hekkert (1991) (OH maser); 31) te Lintel Hekkert et al. (1992) (OH maser); 32) te Lintel Hekkert & Chapman (1996) (OH maser); 33) Vandenbussche et al. (2002) (ISO spectrum).

<sup>s</sup>The central star spectral types are mostly obtained from SIMBAD database, while several of them are updated with following literature: (s1) = Sánchez Contreras et al. (2008); (s2) = Suárez et al. (2006); (s3) = Pereira & Miranda (2007).

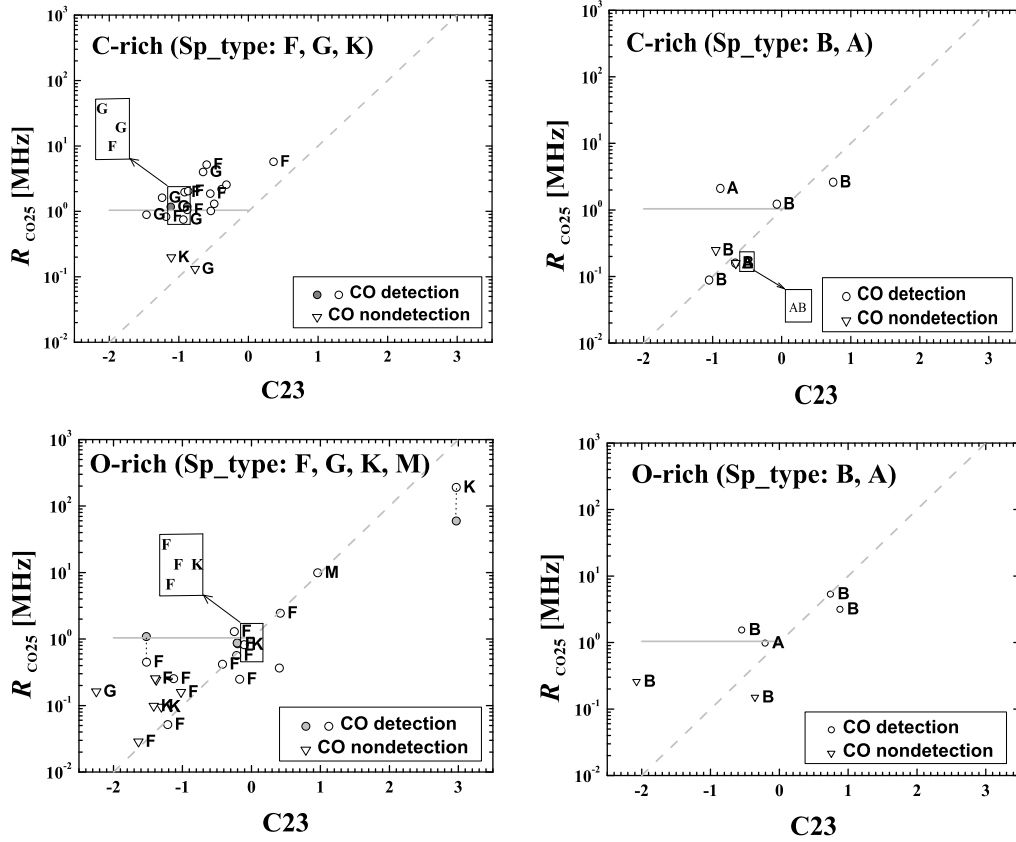


Fig. 5.— The distribution of chemical types and central star spectral types for pAGB stars on the  $R_{\text{CO}25}$ -C23 diagram. The C- and O-rich pAGB objects are plotted in upper and lower panels, while central stars of late spectral types (F, G, K and M) and of early ones (B and A) are plotted in the left and right panels, respectively. The solid and dashed lines are the same as in the left panels of Fig. 2. Crowded regions have been enlarged in rectangles. Gray filled circles are new results from this work. They are connected by vertical line with the corresponding literature CO data, if their differences are obvious.

From point of view of the progenitor mass, a feasible interpretation of the discussed trends is that group-I objects, being predominantly C-rich, are intermediate mass pAGB stars; the group-III sources that are CO-deficient objects are the lowest mass pAGB stars; and the group-II sources are intermediate or high mass stars, which already follow the PNe trend on the CO-IR diagram (see bottom left panel in Fig. 3). This simplified interpretation is supported by the significantly large percentage of O-rich sources (about 70 per cent, see Table 3) among groups-III and II. On the other hand, the paucity of O-rich pAGB stars in group-I region (see the two bottom panels of Fig. 5) seems to suggest that O-rich pAGB stars do not evolve into this region.

From point of view of a single star evolution, we expect that during pAGB stage, the C23 color almost continuously increases with time, while  $F_{25}$  flux generally decreases after a short-lasting increase at the transition phase between AGB and pAGB (see, e.g., Szczerba & Marten 1993; Steffen et al. 1998). Such behavior is due to cooling of circumstellar shell, which is moving away from the central star. However, evolution of the CO 2-1 line flux, another key factor determining the position of a source on the CO-IR diagram, is neither simple nor investigated theoretically to our knowledge. In this respect the CO-IR diagram serves as an observational tool that allows us to put constraints on the CO 2-1 line flux behavior during pAGB phase of stellar evolution.

PNe are well concentrated along the log-linear region (see bottom left panel in Fig. 3) to which ultimately pAGB stars (with exception of the low mass ones that could disperse their circumstellar shells before the onset of photoionization) should evolve. In the frame of single star evolution, the existence of such trend can be understood if the CO 2-1 line flux does not change much during late pAGB (pre-PNe) and PNe phase of evolution, while the  $F_{25}$   $\mu\text{m}$  flux density monotonically decreases. However, in the earlier stages of pAGB evolution, the  $F_{25}$  continuum (see above) and probably also CO 2-1 line fluxes could change non-monotonically, resulting in a relatively complex distribution in Fig. 5 (e.g., the lack of O-rich pAGB sources in group-I and the presence of C-rich ones among group-III).

## 6.2. SED and Binarity

The SEDs of pAGB stars have been classified according to the scheme introduced by van der Veen et al. (1989), with addition of a type 0 (Szczerba et al. 2012). There are six SED types in total: types 0, I, and II, which show significant near infrared (NIR) excess, and types III, IVa, and IVb showing cold dust emission together with a second peak at shorter wavelengths from central star emission. de Ruyter et al. (2006) proposed that the NIR excess, which is seen in the first three SED types (0, I and II) is a signature of gravitationally bounded circumbinary discs perhaps formed during strong binary interaction (van Winckel et al. 2009). The other three SED types (III, IVa and IVb), are signatures of a detached shells and/or expanding tori, which are formed due to mass loss on AGB, or by interaction of AGB star with its companion (Zijlstra 2007), respectively.

Among our CO-IR group-I sources, three quarters (13 out of 17) have SED types of III, IVa or IVb, indicating that their dust emission is dominated by a detached shell/expanding torus. On the other hand, two third (12 out of 18) of the CO-IR group-III pAGB stars have SED types of 0, I or II, showing that they have excess emission from hot dust, a signature of a disc. It is natural to expect that formation of a disc is due to interaction among stars, when primary star was a giant. It is also interesting to note that the pAGB sources that are located in the transition region (those marked by ‘\*’ in Table 3), are showing mostly (8 out of 11) emission from cold (detached) CSEs (with SEDs of type III, IVa, and IVb). The situation in the CO-IR group-II is less evident, as about the same fraction of sources show presence of hot+cold or only cold dust.

Information about binarity is directly obtained from the Torun Catalog of pAGB stars. Although such information is by no means complete in the catalog, some interesting features still can be recognized in the distribution of known binary pAGB stars on the CO-IR diagram, as shown in Fig. 6. First, known binaries appear in all three regions of pAGB stars on CO-IR diagram. However, most of them appear in the CO-deficient region of group-III. In the current sample, about 39 per cent (7 out of 18) group-III pAGB stars are known binaries.

Among the six C-rich stars that belong to group-III, two are known binary systems (Red Rectangle and RV Tau). Binaries are also common in the group-II region (about 40 per cent). What is also striking on Fig. 6 is dichotomy in C23 color distribution of binaries. One, more numerous group, have blue C23 colors (no cold dust), while the second group have red C23 colors (significant amount of cold dust, with Frosty Leo being the most extreme example).

### 6.3. CSE expansion velocity

The CSE expansion velocity of all the 42 pAGB stars with detection of CO 2-1 line show profound trend:  $V_{\text{exp}}$  is smallest among group-III pAGB stars, intermediate among group-I ones and largest among group-II objects. Excluding few exceptional objects, which will be discussed below, we obtain average velocities from the CO line widths for each group:  $12 \pm 2 \text{ km s}^{-1}$  for group-I;  $28 \pm 12 \text{ km s}^{-1}$  for group-II and  $4 \pm 2 \text{ km s}^{-1}$  for group-III. Note that the vast majority of objects located in the transition region (those marked with ‘\*’ in Table 3.) have velocities in between those characteristic for group-I and group-II, with clear exception being IRAS 17106–3046, which have very low  $V_{\text{exp}}$  that is more typical for group-III objects. Because the AGB wind velocity is expected to be higher for more massive AGB stars (see, e.g., the discussions of Nyman et al. 1992), the trend we found suggests that group-II objects are statistically more massive than group-I pAGB stars. On the other hand, so low expansion velocities for group-III objects suggest that CO is observed from circumstellar disks (rotating and/or expanding) rather than from outflows (Bujarrabal et al. 2005, 2013). It is very likely that such disks are formed in binary systems (e.g. van Winckel 2003).

There are two objects in group-I (89 Her and AI Sco), which have very low expansion velocities of their CSE derived from CO lines. Both of them are known to be binaries with 0-type SED, O-rich chemistry, and a blue C23 color close to that typical for O-rich AGB stars. They share characteristics of group-III pAGB objects, but have at the same time a relatively strong CO 2-1 emission in comparison with their  $25 \mu\text{m}$  continuum flux.

The other two group-I objects (IRAS 08005–2356 and IRAS 23541+7031), on the other hand, have very high expansion velocities, much larger even

than those typical for group-II pAGB objects. IRAS 08005–2356 has a broad CO line, which was only tentatively detected by Hu et al. (1994). However, similarly high velocities are also detected in optical spectrum of this star by Slijkhuis et al. (1991), and Sánchez Contreras et al. (2008), which may be interpreted as a signature of ongoing fast wind (or jet) from this source. Its type-I SED indicates significant near infrared emission, which may be interpreted as emission from hot dust in a disc, but its  $R_{\text{CO}25} = 5.20$  is the largest among group-I pAGB stars. IRAS 23541+7031 has a disk or torus of molecular gas, which seems to be expanding (Castro-Carrizo et al. 2002). It has very rich and complex wind activity and rapidly evolving shocked material (Sánchez Contreras et al. 2010). In this respect, a broad CO 2-1 line detected by Hajian et al. (1996) is not surprising.

Roberts 22 and IRAS 17245-3951 (Walnut Nebula) are another two special objects with normal or high CSE expansion velocities ( $31$  and  $15 \text{ km s}^{-1}$ , respectively), but this time being members of our group-III objects ( $R_{\text{CO}25} = 0.16$  and  $0.25$ , respectively). Again, the broad CO lines may be interpreted by the contribution from bipolar outflows, because both show typical bipolar nebulae. We note that Roberts 22 was known to show broadened  $H_{\alpha}$  emission line and was thus suspected to be a Wolf-Rayet star (Roberts 1962).

### 6.4. Post-AGB sub-types

Finally, we would like to put attention to the fact that, among sources from Table 3, there are two pAGB classes (Szczerba et al. 2007) that are the most abundant. They are ‘21 micron’ sources (12 objects) and RV Tau stars (8 sources). These two groups have quite well defined properties. The ‘21 micron’ sources are a group of C-rich intermediate mass stars with the still unidentified  $21 \mu\text{m}$  dust feature (Kwok et al. 1989), which also show s-process elements enhancement (Van Winckel & Reyniers 2000), and have periodic variability well correlated with their effective temperature (Hrivnak et al. 2010). RV Tau stars are luminous variable stars, which show alternating deep and shallow minima with periods between 30 and 150 days, and spectral types F, G and K (e.g. Preston et al. 1963). Most of them show IR excess, which is interpreted as a remnant of AGB mass loss (Jura 1986). RV Tau stars with near-IR



excess (very likely due to radiation from disks) are probably binaries (de Ruyter et al. 2005).

These two groups have well established positions on the CO-IR diagram. Almost all members of the ‘21  $\mu\text{m}$ ’ type sources from our sample are in our group-I, with one belonging to the transition region and only one to group-III (IRAS 19477+2401). It is remarkable that 10 (out of 17, or 59 per cent) objects in group-I are ‘21  $\mu\text{m}$ ’ sources. Their IR colors are in the range  $-1.3 < \text{C23} < -0.55$ . All but one have a G or F spectral type, 9 (among 12) have a SED of IVa or IVb type, none of them is known to be binary, their outflow velocities are around  $10 \text{ km s}^{-1}$  (with an average of  $12 \pm 3 \text{ km s}^{-1}$ ).

On the other hand, 7 (out of 8) RV Tau stars from our sample belong to group-III objects, with only one source (AI Sco) being a member of group-I on the CO-IR diagram. This is not so surprising since RV Tau variables are well-known to be CO-deficient stars (Alcolea & Bujarrabal 1991). RV Tau stars from our sample consist of the majority of the blue part of the group-III objects, with IR colors in a narrow range of  $-1.5 < \text{C23} < -1.1$ . They have O-rich chemistry, 7 (out of 8) have SED classified as 0 or I (with AR Pup being the only exception with SED of type-III), 7 of them are also known binaries (with the only exception of AI CMi, which do not have near-IR excess - see e.g. SED in the Torun catalog), and the three RV Tau variables with detected CO 2-1 line all show very narrow CO lines (with  $V_{\text{exp}} = 1.5 \sim 5.6 \text{ km s}^{-1}$ ).

### 6.5. Overall properties of the CO-IR groups of post-AGB stars

We summarize below the properties of the different groups of pAGB objects, as inferred from the above discussion. The key features of each CO-IR group are collected in Table 4 and illustrated in a cartoon (Fig. 7).

#### 6.5.1. Group-I

The group-I pAGB stars have a relatively narrow range of  $R_{\text{CO25}}$  ratios from 0.42 to 5.2 MHz, with a median of  $\sim 1 \text{ MHz}$  and C23 color varying between -1.5 and -0.5. They represent the early pAGB stage of intermediate mass pAGB stars, because of their F to G spectral types and C-rich chemistry. This group contains almost all of the

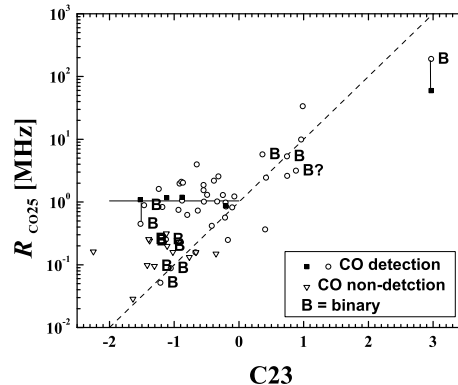


Fig. 6.— The distribution of binary pAGB stars (marked as ‘B’) on the CO-IR diagram. Only group-III contains some CO non-detections. The solid and dashed lines represent the distribution trends of groups-I, II and III.

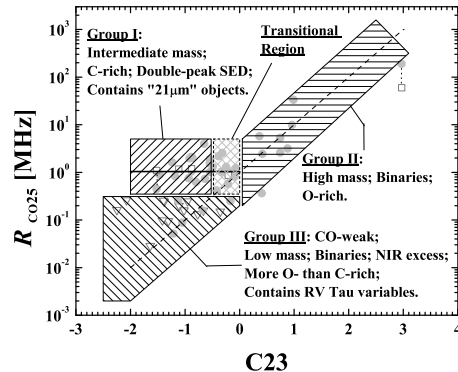


Fig. 7.— The cartoon illustrates the main regions and the key features of the three pAGB CO-IR groups. Observed pAGB stars are shown as gray points.

TABLE 4  
SUMMARY OF THE BULK PROPERTIES OF THE THREE CO-IR GROUPS.

Group	C23	$R_{CO25}$	Chemistry	Sp.Type	Binary	SED.Type	$V_{exp}$ $km\ s^{-1}$	Special objects
I	-1.52 ~ -0.5	0.42 ~ 5.2	C	F, G	7%	III,IVa,IVb	$12 \pm 2$	21 $\mu m$ objects
II	+0.36 ~ +2.97	0.37 ~ 59.62	O or C	K to B	44%	0,II,III,IVb	$28 \pm 12$	
III	-2.25 ~ -0.17	< 0.26	O	M to B	39%	0,I,II	$4 \pm 2$	RV Tau variables

considered ‘21  $\mu m$ ’ objects.

### 6.5.2. Group-II

The group-II pAGB stars are the reddest objects in our sample. They are distributed along a log-linear trend on the CO-IR diagram, which coincides with a similar trend of PNe. On average, group-II objects are more massive pAGB stars than group-I sources, due to their higher  $V_{exp}$ . However, this region should also contain evolved intermediate mass pAGB stars that are approaching PNe phase.

### 6.5.3. Group-III

The group-III pAGB objects are those with similar C23 colors as group-I objects but with much weaker CO 2-1 line. They are probably the lowest mass pAGB stars, predominantly O-rich, with very high percentage of known binaries, which is in agreement with their type-0, I and II SED (near-IR excess). Most of the RV Tau variables are in this group.

### 6.5.4. Transition region

The objects in this region have C23 colors intermediate between groups-I and II. They are predominantly O-rich as group-II objects, but have  $R_{CO25}$  ratios similar as group-I objects. Their CSE expansion velocities are also intermediate between the two groups.

## 7. SUMMARY

A survey of CO 2-1 line has been performed toward 58 known high Galactic latitude pAGB stars. Circumstellar CO lines were detected only toward five of these objects, with one new detection. The detected line profiles show various features such as line wings, absorption features and triangular peak.

To complete our survey, we performed a compilation of literature reporting single dish CO 2-1 line observation for all 393 pAGB stars (likely, RCrB-eHe-LTP and RV Tau types from the Torun Catalog of pAGB stars). We found observations for 133 pAGB stars (34 per cent of all objects in the Torun Catalog). The CO 2-1 line has been detected in 44 objects among them. The CO 2-1 line data for AGB stars and PNe were also compiled for comparison.

CO-IR flux ratio  $R_{CO25}$  is defined using the integrated CO 2-1 line flux and *IRAS* 25 $\mu m$  flux density. This ratio is compared with IR color C23 that is defined with the *IRAS* 60 to 25 $\mu m$  flux ratio. So constructed CO-IR diagram is used to investigate the pAGB phase of stellar evolution.

Post-AGB stars segregate into three groups on the CO-IR diagram: group-I pAGB stars show a narrow range of  $R_{CO25}$  ratios that are independent of the C23 colors (Eq. 2); groups-II pAGB stars have redder C23 colors and usually larger  $R_{CO25}$  ratios; group-III pAGB stars have significantly smaller  $R_{CO25}$  ratios (weak CO lines).

Comparison of the pAGB stars with AGB stars and PNe on the CO-IR diagram reveals that post AGB objects are really located between the AGB stars and PNe. Planetary nebulae show a profound trend on the CO-IR diagram which agrees well with the trend of group-II pAGB stars.

Combining these features with various properties such as chemical types, central star spectral types, binarity, SED types, CSE expansion velocities and pAGB sub-types (defined in the Torun Catalog) of the pAGB stars, the three pAGB CO-IR groups are found to have distinctive characteristics related to mass, evolutionary stage and binarity.

The CO-IR diagram is proven to be a powerful tool to discriminate the different effects of stellar mass, evolution and binarity of pAGB stars and

to investigate the co-evolution of circumstellar gas and dust during the fast post-AGB stage.

This research has intensively made use of NASA's Astrophysics Data System Bibliographic Services and SIMBAD database, operated at CDS, Strasbourg, France. We thank ARO telescope operators for the assistance in remote observations. The SMT is operated by the Arizona Radio Observatory (ARO), Steward Observatory, University of Arizona. J.H. thanks Dr. T.M., Dame for kindly offering additional information from their Galactic CO 1-0 line survey to help us identify possible interstellar contamination .

This work benefited from the collaboration among the coauthors funded by Marie Curie Actions International Research Staff Exchange Scheme (project No. 269193) of European Union. J.H. also thanks the projects (No. 11173056 and 11033008) of the National Natural Science Foundation of China. R.Sz. and M.S. acknowledge the support from grants 2011/01/B/ST9/02031 and 2011/01/B/ST9/02229. T.I. acknowledges the support from NSC grant NSC 96-2112-M-001-018-MY3.

*Facilities:* HHT ().

**A. COMPILATION OF LITERATURE CO 2-1 LINE DATA FOR AGB, pAGB STARS AND PNe**

Table 5: Literature CO 2-1 line data of post-AGB stars.

IRAS	Other name	Chem	Tp( $\sigma$ ) mK	NoteT <sup>a</sup>	I( $\sigma$ ) K km s <sup>-1</sup>	V <sub>sys</sub> ( $\sigma$ ) km s <sup>-1</sup>	V <sub>exp</sub> ( $\sigma$ ) km s <sup>-1</sup>	Tel <sup>b</sup>	Tscale	Obs.mode <sup>c</sup>	Obs.Date yyyy-mm-dd	Literature
	CRL 2688		1300					OVRO	TA*	S	1978-03,04	1979ApJ...230..149W
	CRL 2688	C	2300 (500)					OVRO	TA*	MapC	1978-11 to 12,1979-11 to 12	1982ApJ...252..616K
	CRL 2688		4200					ARO12m	TA*	S	1985-02,04	1987ApJ...319..367W
	CRL 2688				185 (2)	-36.0	17.9(2.3)	IRAM30m	Tmb	S	1988-08	1992A&A...256..235
	CRL 2688				312.5(1.3)	-35.6	60	IRAM30m	Tmb	S	1991-06	1997A&A...324.1123
	CRL 2688		5890 (20)		151.7	-35.7	31	JCMT	TA*	S	1995-05	1997A&A...327..342
	CRL 2688				312.5			IRAM30m	Tmb	S	1996-11,1997-05	2000A&A...355..69
	CRL 2688	C	16670 (200)	Jy/K				IRAM30m	Tmb	S	2000-09	2002ApJ...577..961H
	HD 107369		(23)					SEST	Tmb	S	1989-05,1990-07	1993A&A...269..231
	V4334 Sgr		(50)					JCMT	TA*	S	1997-06-29	1998A&A...335..292
01005+7910			(16)					IRAM30m	Tmb	S	1989-01	1993A&A...267..515
01005+7910	C		(248)	cont				SMT10m	Tmb	S	1999-12-03 to 2000-02-04	2005ApJ...624..331H
02143+5852			(14)	cont				IRAM30m	Tmb	S	1989-01	1993A&A...267..515
02143+5852			(50)					SMT10m	Tmb	S	1999-12-03 to 2000-02-04	2005ApJ...624..331H
04166+5719	TW Cam	O	(400)					IRAM30m	Tmb	S	1989-04 to 06	1991A&A...245..499
04296+3429			400			-62.3	15.6	JCMT	TR*	S	1988-12	1990A&A...228..503
04296+3429	C	450 (128)			8.3	-66	12.0	IRAM30m	Tmb	MapC	1989-01	1993A&A...267..515
04296+3429	C	70 (17)			1.12	-64.8	10.8	SMT10m	Tmb	S	1999-12-03 to 2000-02-04	2005ApJ...624..331H
04395+3601	CRL 618	C	2100 (800)					OVRO	TA*	MapC	1978-11 to 12,1979-11 to 12	1982ApJ...252..616K
04395+3601	CRL 618		2000					ARO12m	TA*	S	1985-02,04	1987ApJ...319..367W
04395+3601	CRL 618		2200 (150)		53.9	-22	18	ARO12m	Tmb	S	1985-12 to 1988-01	1989ApJ...346..201H
04395+3601	CRL 618		3500 (90)			-21.7(0.3)	18.6(0.4)	ARO12m	TA*	S	1987-01-13 to 16	1990ApJ...358..251W
04395+3601	CRL 618		9300 (160)		250.0	-21.9	11.6	IRAM30m	Tmb	MapC	1987-02	1988A&A...196L...5
04395+3601	CRL 618				161 (1)	-21.4	18.5(1.7)	IRAM30m	Tmb	S	1988-08	1992A&A...256..235
04395+3601	CRL 618		8640	2C	270.0(3.4)	-21.9(0.2)	18.2(0.5)	IRAM30m	Tmb	S	1988-08	1989A&A...222L...1
04395+3601	CRL 618		5160 (200)	2C		-22.6(1.0)	19.1(0.8)	CSO	Tmb	S	1988-08,1989-11	1989ApJ...345L..87G
04395+3601	CRL 618				182.2(1.1)	-21.5	40	IRAM30m	Tmb	S	1991-06	1997A&A...324.1123
04395+3601	CRL 618				46.2 (5.1)			ARO12m	Tmb	MapC	1994-11-30	1998ApJ...509..392M
04395+3601	CRL 618				182.2			IRAM30m	Tmb	S	1996-11,1997-05	2000A&A...355..69
04395+3601	CRL 618	C	2400 (90)		60.0 (0.8)	-22.0	23.9	ARO12m	Tmb	S	1997-05,1997-12	2002ApJ...572..326B
04395+3601	CRL 618	C	11190	Jy/K				IRAM30m	Tmb	S	2000-09	2002ApJ...577..961H
04440+2605	RV Tau		(37)					ARO12m	TA*	S	1987-01-13 to 16	1990ApJ...358..251W
04440+2605	RV Tau		(60)					IRAM30m	Tmb	S	1988-06	1988A&A...206L..17
04440+2605	RV Tau	O	(30)					IRAM30m	Tmb	S	1989-04 to 06	1991A&A...245..499
05338-3051	RV Col		(200)					SEST	Tmb	S	1989-05,1990-07	1993A&A...269..231
06034+1354	DY Ori		(30)					IRAM30m	Tmb	S	1989-04 to 06	1991A&A...245..499
06072+0953	CT Ori		(40)					IRAM30m	Tmb	S	1989-04 to 06	1991A&A...245..499
06108+2743	SU Gem		(26)					ARO12m	TA*	S	1987-01-13 to 16	1990ApJ...358..251W
06108+2743	SU Gem	O	(100)					IRAM30m	Tmb	S	1989-04 to 06	1991A&A...245..499
06176-1036	Red Rectangle		(160)					ARO12m	Tmb	S	1984-12	1986ApJ...304..394Z
06176-1036	Red Rectangle		1500	hand	6.6	+0.5	2.2	IRAM30m	Tmb	S	1993-04	1995ApJ...453..721J
06176-1036	Red Rectangle		(18)		1.36	-1	11	ARO12m	Tmb	S	1994-01	1996ApJ...472..703D
06176-1036	Red Rectangle		260 (20)		1.80	+0.2	9	JCMT	TA*	S	1995-05	1997A&A...327..342
06530-0213			610 (110)		7.0	+33	10	SEST	Tmb	S	1991-04	1994A&AS...103..301
06530-0213		C	120 (12)		2.47	+31.4	12.5	SMT10m	Tmb	S	1999-12-03 to 2000-02-04	2005ApJ...624..331H
07134+1005	HD 56126	C	3210 (97)		43.9	+73	10.2	IRAM30m	Tmb	S	1989-01	1993A&A...267..515
07134+1005	HD 56126	C	2200 (100)		28	+73		IRAM30m	Tmb	MapC	1990-04 to 06,1991-01	1992A&A...257..701
07134+1005	HD 56126	C	640 (70)		9.2 (0.9)	+73.0(0.8)	10.7(1.1)	CSO	Tmb	S	1996-12-28 to 1997-01-02	1998ApJS...117..209K
07134+1005	HD 56126	C	630 (5)		9.03	+73.5	10.6	SMT10m	Tmb	S	1999-12-03 to 2000-02-04	2005ApJ...624..331H
07284-0940	U Mon		(33)					ARO12m	TA*	S	1987-01-13 to 16	1990ApJ...358..251W

Note: Repeated observations of the same object are listed as separate entries. Our observations of high Galactic latitude pAGB objects are not included.

Table 5: (continued)

IRAS	Other name	Chem	Tp( $\sigma$ ) mK	NoteT <sup>a</sup>	I( $\sigma$ ) K km s <sup>-1</sup>	V <sub>sys</sub> ( $\sigma$ ) km s <sup>-1</sup>	V <sub>exp</sub> ( $\sigma$ ) km s <sup>-1</sup>	Tel <sup>b</sup>	Tscale	Obs.mode <sup>c</sup>	Obs.Date yyyy-mm-dd	Literature
07284-0940	U Mon		(150)					IRAM30m	Tmb	S	1988-06	1988A&A...206L..17
07284-0940	U Mon	O	(70)					IRAM30m	Tmb	S	1989-04 to 06	1991A&A...245..499
07331+0021	AI CMi	O	(56)					IRAM30m	Tmb	S	1989-01	1993A&A...267..515
07399-1435	OH231.8+4.2	O	3600	hand		+33	30 (5)	SEST	Tmb	MapC	1996-11	1997A&A...327..689
07399-1435	OH231.8+4.2	O	580 (20)			+36.2(2.6)	41.6(2.6)	SMT10m	TA*	S	2003-10 to 2007-06	2009ApJ...690..837M
07430+1115			(90)					IRAM30m	Tmb	S	1989-01	1993A&A...267..515
07430+1115		C	(13)					SMT10m	Tmb	S	1999-12-03 to 2000-02-04	2005ApJ...624..331H
08005-2356			120 (60)		14	+50	100	SEST	Tmb	S	1991-04	1994A&AS..103..301
08011-3627	AR Pup	O	(200)					IRAM30m	Tmb	S	1989-04 to 06	1991A&A...245..499
08187-1905	HD 70379		(18)					SMT10m	Tmb	S	1999-12-03 to 2000-02-04	2005ApJ...624..331H
08544-4431	V390 Vel	C	140 (10)		1.2	+45.6	8.0	SEST	Tmb	S	1999-10,2001-03	2002A&A...390..501
08544-4431	V390 Vel				3.0	+61.3	6.4	SEST	Tmb	S	1999-10-02,2000-07-28	1991A&A...242..247
09032-3953			180 (60)		6.7	+36	25	SEST	Tmb	S	1991-04	1994A&AS..103..301
09370-4826			(160)					SEST	Tmb	S	1991-04	1994A&AS..103..301
09371+1212	FROSTY LEONIS		176 (7)			-5.6 (0.4)	36.6(0.5)	ARO12m	TA*	S	1987-01-13 to 16	1990ApJ...358..251W
10158-2844	HR 4049		(200)					SEST	Tmb	S	1989-05,1990-07	1993A&A...269..231
10158-2844	HR 4049	C	(40)					IRAM30m	Tmb	S	1990-04 to 06,1991-01	1992A&A...257..701
10178-5958	Hen 3-401		190 (30)		5.2	-29.0	15	SEST	Tmb	S	19??-09-01 to 04	1991A&A...242..247
10194-5625			(160)					SEST	Tmb	S	1991-04	1994A&AS..103..301
10197-5750	Roberts 22		150 (40)		9.0	-0.1		SEST	Tmb	S	19??-09-01 to 04	1991A&A...242..247
11000-6153	HD 95767		(200)					SEST	Tmb	S	1989-05,1990-07	1993A&A...269..231
11381-6401			(190)					SEST	Tmb	S	1991-04	1994A&AS..103..301
11385-5517	HD 101584	O	300		41.3	+44	145.	SEST	Tmb	MapC	1997-08	1999A&A...347..194
11544-6408			(140)					SEST	Tmb	S	1991-04	1994A&AS..103..301
12067-4508	HD 105578		(200)					SEST	Tmb	S	1989-05,1990-07	1993A&A...269..231
12222-4652	HD 108015		(200)					SEST	Tmb	S	1989-05,1990-07	1993A&A...269..231
12419-5414	Boomerang Nebula		160	hand		-10	35	SEST	Tmb	MapC	1994-08,1995-08 to 1995-10	1997ApJ...487L.155S
12419-5414	Boomerang Nebula		150 (20)		5.0	-3.5		SEST	Tmb	S	19??-09-01 to 04	1991A&A...242..247
14488-5405	CPD -53 5736		90		2.07	-10	10.0	SEST	Tmb	S	1998 to 2002	2005A&A...429..977
14524-6838	HD 131356		(200)					SEST	Tmb	S	1989-05,1990-07	1993A&A...269..231
15465+2818	R CrB		(100)					ARO12m	Tmb	S	1984-12	1986ApJ...304..394Z
15465+2818	R CrB		(41)					ARO12m	TA*	S	1987-01-13 to 16	1990ApJ...358..251W
16342-3814	OH 344.1 +5.8	O	29 (7)		2.14 (0.14)	+44 (1)	46 (1)	SMT10m	Tmb	S	2008-05-09	2008A&A...488L..21
16594-4656			1750		32.60	-25	10.0	SEST	Tmb	S	1998 to 2002	2005A&A...429..977
17106-3046			300		1.84	0	2	SEST	Tmb	S	1998 to 2002	2005A&A...429..977
17150-3224	RAFGL 6815		1000 (300)		18.6	+15	15	JCMT	Tmb	S	1990-11,12	1994A&AS..103..301
17150-3224	RAFGL 6815	O	1000			+15	15	JCMT	Tmb	S	1990-12	1993A&A...273..185
17150-3224	RAFGL 6815		650		12.84	+15		SEST	Tmb	S	1998 to 2002	2005A&A...429..977
17245-3951	OH348.8-2.8		40		0.58	0	15	SEST	Tmb	S	1998 to 2002	2005A&A...429..977
17423-1755	Hen 3-1475		280 (40)		15.9 (0.5)	+47.5(0.9)	53 (2)	IRAM30m	Tmb	S	1997-09	2004A&A...414..581
17436+5003	V814 Her		370			-37.5	7.7	ARO12m	Tmb	S	1986-04,1987-04	1989A&A...209..119
17436+5003	V814 Her		1800		33	-35.5	13.2	IRAM30m	Tmb	S	1987-10	1991A&A...246..153
17436+5003	V814 Her	O	2000 (40)		36.1	-35		IRAM30m	Tmb	MapC	1990-04 to 06,1991-01	1992A&A...257..701
17436+5003	V814 Her	O	1500		29.3	-34.7	11.7	IRAM30m	Tmb	S	1993-08	1998A&AS..130...1
17436+5003	V814 Her	O	230 (6)		4.24	-34.8	13.8	SMT10m	Tmb	S	1999-12-03 to 2000-02-04	2005ApJ...624..331H
17441-2411	AFGL 5385		670 (160)		8.3	+5	15	SEST	Tmb	S	1991-04	1994A&AS..103..301
17441-2411	AFGL 5385		570		6.24	+110		SEST	Tmb	S	1998 to 2002	2005A&A...429..977
17530-3348	AI Sco		(600)					IRAM30m	Tmb	S	1988-06	1988A&A...206L..17
17530-3348	AI Sco	O	300 (100)		1.8	-37		IRAM30m	Tmb	S	1989-04 to 06	1991A&A...245..499
17534+2603	89 Her		600		4.1	-7.9	3.2	IRAM30m	Tmb	S	1987-10	1991A&A...246..153

Table 5: (continued)

IRAS	Other name	Chem	Tp( $\sigma$ ) mK	Note <sup>T<sup>a</sup></sup>	I( $\sigma$ ) K km s <sup>-1</sup>	V <sub>sys</sub> ( $\sigma$ ) km s <sup>-1</sup>	V <sub>exp</sub> ( $\sigma$ ) km s <sup>-1</sup>	Tel <sup>b</sup>	Tscale	Obs.mode <sup>c</sup>	Obs.Date yyyy-mm-dd	Literature
17534+2603	89 Her		1000 (70)		4.6	-7.9	4	IRAM30m	Tmb	S	1989-04 to 06	1991A&A...245..499
17534+2603	89 Her		200 (50)					SMT10m	TA*	S	2003-10 to 2007-06	2009ApJ...690..837M
18025-3906			(130)					SEST	Tmb	S	1991-04	1994A&AS..103..301
18095+2704		O	(30)					IRAM30m	Tmb	S	1990-04 to 06,1991-01	1992A&A...257..701
18276-1431	OH17.7-2.0		(100)					CSO	TA*	S	1987-07	1989ApJ...336..822K
18276-1431	OH17.7-2.0	O	1000 (170)		19.2 (1.0)	+61.6	12.2	IRAM30m	Tmb	S	1988-02	1990A&A...239..173
18281+2149	AC Her		(20)					ARO12m	TA*	S	1987-01-13 to 16	1990ApJ...358..251W
18281+2149	AC Her		200		0.7			IRAM30m	Tmb	S	1988-06	1988A&A...206L..17
18281+2149	AC Her	C	100 (300)		0.5	-10		IRAM30m	Tmb	S	1989-04 to 06	1991A&A...245..499
18372-2257	V348 Sgr		(150)					SEST	Tmb	S	1989-05,1990-07	1993A&A...269..231
18415-2100	MV Sgr		(200)					SEST	Tmb	S	1989-05,1990-07	1993A&A...269..231
19114+0002	AFGL 2343		380			+94.3	33.7	ARO12m	Tmb	S	1986-04,1987-04	1989A&A...209..119
19114+0002	AFGL 2343	O	2520 (107)		126.8	+99	33.7	IRAM30m	Tmb	S	1989-01	1993A&A...267..515
19114+0002	AFGL 2343		470 (70)		22.8 (0.5)	+99.0(0.2)	28.1(0.2)	SEST	Tmb	S	1989-05,1990-07	1993A&A...269..231
19114+0002	AFGL 2343	O	3400 (100)		171	+99		IRAM30m	Tmb	MapC	1990-04 to 06,1991-01	1992A&A...257..701
19114+0002	AFGL 2343	O	3450 (80)		172.4	+97	37	IRAM30m	Tmb	MapC	1999-08	2001A&A...367..826
19132-3336	RY Sgr		(300)					SEST	Tmb	S	1989-05,1990-07	1993A&A...269..231
19306+1407			(77)					IRAM30m	Tmb	S	1989-01	1993A&A...267..515
19343+2926	PN M1-92	O	1100		56.6	+0.3	32.5	IRAM30m	Tmb	S	1990-10	1998A&AS..130....1
19374+2359			(123)	cont				IRAM30m	Tmb	S	1989-01	1993A&A...267..515
19374+2359			(200)					JCMT	Tmb	S	1990-11,12	1994A&AS..103..301
19386+0155			(63)					IRAM30m	Tmb	S	1990-07	1993A&A...267..515
19454+2920			730		14.3	+21.4	14.5	IRAM30m	Tmb	S	1988-01	1991A&A...246..153
19454+2920		C	730 (41)		14.3	+21	14.5	IRAM30m	Tmb	MapC	1989-01	1993A&A...267..515
19454+2920			210		3.8	+19.7	17.8	JCMT	TA*	S	1991-10-25 to 27	1993ApJ...402..292V
19475+3119	HD 331319		770		15	+17.7	14.6	IRAM30m	Tmb	S	1989-01	1991A&A...246..153
19475+3119	HD 331319		720 (62)		14.9	+18	14.5	IRAM30m	Tmb	MapC	1989-01	1993A&A...267..515
19475+3119	HD 331319	O	160 (7)		3.51	+18.4	16.2	SMT10m	Tmb	S	1999-12-03 to 2000-02-04	2005ApJ...624..331H
19477+2401			(10)	cont				SMT10m	Tmb	S	1999-12-03 to 2000-02-04	2005ApJ...624..331H
19480+2504			600		13	+41.7	15.4	IRAM30m	Tmb	S	1989-01	1991A&A...246..153
19480+2504		C	610 (54)		12.8	+42	12.3	IRAM30m	Tmb	S	1989-01	1993A&A...267..515
19480+2504		C	470 (94)		9.8	+41	15.4	IRAM30m	Tmb	MapC	1990-07	1993A&A...267..515
19480+2504			170		5.8	+42.0	27.0	JCMT	TA*	S	1991-10-25 to 27	1993ApJ...402..292V
19486+1350	TW Aql	O	(60)					IRAM30m	Tmb	S	1989-04 to 06	1991A&A...245..499
19500-1709	HD 187885		300 (70)		3.8 (0.3)	+25	8	CSO	TA*	S	1987-07	1989ApJ...336..822K
19500-1709	HD 187885		1230 (45)		27.7	+25	12.0	IRAM30m	Tmb	MapC	1989-01	1993A&A...267..515
19500-1709	HD 187885		390 (40)		7.0 (0.2)	+26.0(0.3)	13.2(0.5)	SEST	Tmb	S	1989-05,1990-07	1993A&A...269..231
19500-1709	HD 187885	C	1900 (100)		48	+24		IRAM30m	Tmb	MapC	1990-04 to 06,1991-01	1992A&A...257..701
19500-1709	HD 187885		1360 (51)		23.1	+24	12.8	IRAM30m	Tmb	S	1990-07	1993A&A...267..515
19500-1709	HD 187885		1100		22.0	+25.0		IRAM30m	Tmb	S	1990-10	1998A&AS..130....1
19500-1709	HD 187885	C	190 (6)		4.41	+25.0	17.2	SMT10m	Tmb	S	1999-12-03 to 2000-02-04	2005ApJ...624..331H
19590-1249	LS IV -12 111	O	(17)					SMT10m	Tmb	S	1999-12-03 to 2000-02-04	2005ApJ...624..331H
20000+3239			700		9.4	+13.5	12.3	IRAM30m	Tmb	S	1989-01	1991A&A...246..153
20000+3239		C	550 (64)	cont	9.5	+14	12.0	IRAM30m	Tmb	MapC	1989-01	1993A&A...267..515
20004+2955	V1027 Cyg	O	(50)					IRAM30m	Tmb	S	1990-04 to 06,1991-01	1992A&A...257..701
20028+3910	PN PM 2-43		160			+4.2	10.5	ARO12m	Tmb	S	1984-12	1986ApJ...304..394Z
20028+3910	PN PM 2-43		750		14.9	+5.9	16.0	IRAM30m	Tmb	S	1989-01	1991A&A...246..153
20028+3910	PN PM 2-43		700 (40)		15.1	+6	17.5	IRAM30m	Tmb	MapC	1989-01	1993A&A...267..515
20028+3910	PN PM 2-43		900		17.7	+4.0	15.6	IRAM30m	Tmb	S	1993-08	1998A&AS..130....1
20028+3910	PN PM 2-43		130 (11)		2.53	+6.2	13.0	SMT10m	Tmb	S	1999-12-03 to 2000-02-04	2005ApJ...624..331H

Table 5: (continued)

IRAS	Other name	Chem	Tp( $\sigma$ ) mK	Note <sup>a</sup>	T( $\sigma$ ) K	$V_{\text{sys}}(\sigma)$ km s <sup>-1</sup>	$V_{\text{exp}}(\sigma)$ km s <sup>-1</sup>	Tel <sup>b</sup>	Tscale	Obs.mode <sup>c</sup>	Obs.Date yyyy-mm-dd	Literature
20117+1634	R Sge	O	(100)					IRAM30m	Tmb	S	1989-04 to 06	1991A&A...245..499
20343+2625	V Vul	O	(30)					IRAM30m	Tmb	S	1989-04 to 06	1991A&A...245..499
20462+3416	LS II +34 26		(15)					SMT10m	Tmb	S	1999-12-03 to 2000-02-04	2005ApJ...624..331H
20572+4919			(14)	cont				SMT10m	Tmb	S	1999-12-03 to 2000-02-04	2005ApJ...624..331H
21537+6435			(180)					JCMT	Tmb	S	1990-11,12	1994A&AS..103..301
22023+5249			(80)					IRAM30m	Tmb	S	1989-01	1993A&A...267..515
22223+4327			(300)					IRAM30m	Tmb	S	1988-01	1991A&A...246..153
22223+4327		C	640 (32)		12.3	-30	14.0	IRAM30m	Tmb	MapC	1989-01	1993A&A...267..515
22272+5435	HD 235858		3100			-28.0	9.6	JCMT	TR*	S	1988-12	1990A&A...228..503
22272+5435	HD 235858	C	6270 (55)		80.5	-28	11.8	IRAM30m	Tmb	MapC	1989-01	1993A&A...267..515
22272+5435	HD 235858	C	6030 (119)		76.3	-29	9.5	IRAM30m	Tmb	MapC	1990-07	1993A&A...267..515
22272+5435	HD 235858	C	5300		125.6	-28.4	10.4	IRAM30m	Tmb	S	1991-05	1998A&AS..130....1
22272+5435	HD 235858	C	1120 (8)		13.6	-28.1	9.1	SMT10m	Tmb	S	1999-12-03 to 2000-02-04	2005ApJ...624..331H
22327-1731	HD213985	C	(70)					IRAM30m	Tmb	S	1990-04 to 06,1991-01	1992A&A...257..701
22574+6609			500		11	-64.0	15	IRAM30m	Tmb	S	1988-01	1991A&A...246..153
22574+6609		C	60 (18)		1.95	-61.7	24.6	SMT10m	Tmb	S	1999-12-03 to 2000-02-04	2005ApJ...624..331H
23304+6147			1600		25	-16.1	11.5	IRAM30m	Tmb	S	1988-01	1991A&A...246..153
23304+6147			700			-15.9	15.5	JCMT	TR*	S	1988-12	1990A&A...228..503
23304+6147		C	200 (8)		2.92	-16.6	9.2	SMT10m	Tmb	S	1999-12-03 to 2000-02-04	2005ApJ...624..331H
23321+6545	PN PM 2-48		270 (110)		7.5 (0.6)	-59	15	CSO	TA*	S	1987-07	1989ApJ...336..822K
23321+6545	PN PM 2-48		1200		28	-55.2	17.0	IRAM30m	Tmb	S	1989-01	1991A&A...246..153
23321+6545	PN PM 2-48	C	1400		27.0	-53.7	14.3	IRAM30m	Tmb	S	1991-05	1998A&AS..130....1
23321+6545	PN PM 2-48		370		7.1	-55.3	18.2	JCMT	TA*	S	1991-10-25 to 27	1993ApJ...402..292V
23541+7031	PK 118+08.1		470		25.3	-27	54	IRAM30m	Tmb	S	1989-10 to 1993-05	1996ApJ...467..341H
Z02229+6208		C	480 (6)		6.96	+24.1	10.7	SMT10m	Tmb	S	1999-12-03 to 2000-02-04	2005ApJ...624..331H

<sup>a</sup> cont = interstellar contamination; Jy/K = line peak temperature converted back from line peak flux in Jy; hand = line peak temperature measured by hand from published spectral plots; 2C = line peak temperature as the sum of a two components fit.

<sup>b</sup> Telescopes for CO observations: ARO12m = ARO 12 m telescope at Kitt Peak; CSO = the 10.4 m Robert B. Leighton telescope of the Caltech Submillimeter Observatory on Mauna Kea, Hawaii; IRAM30m = IRAM 30m telescope at Pico Veleta; JCMT = 15 m James Clerk Maxwell Telescope on Mauna Kea, Hawaii; OVRO = the Caltech 10m telescope at the Owens Valley Radio Observatory; SEST = the 15 m Swedish-ESO Submillimetre Telescope on La Silla, Chile; SMT10m = the 10 m Sub-Millimeter Telescope on Mt. Graham, AZ.

<sup>c</sup> Observation modes: S = single point; Map = single dish map center.



Table 6: List of literature for Table 5.

1979ApJ...230..149W	Wannier et al. (1979)	1995ApJ...453..721J	Jura et al. (1995)
1982ApJ...252..616K	Knapp et al. (1982)	1996ApJ...467..341H	Hajian et al. (1996)
1986ApJ...304..394Z	Zuckerman & Dyck (1986a)	1996ApJ...472..703D	Dayal & Biegging (1996)
1987ApJ...319..367W	Wannier & Sahai (1987)	1997A&A...324.1123B	Bachiller et al. (1997)
1988A&A...196L...5B	Bachiller et al. (1988)	1997A&A...327..342G	Greaves & Holland (1997)
1988A&A...206L..17B	Bujarrabal et al. (1988)	1997A&A...327..689S	Sánchez Contreras et al. (1997)
1989A&A...209..119Z	Zuckerman & Dyck (1989)	1997ApJ...487L.155S	Sahai & Nyman (1997)
1989A&A...222L...1C	Cernicharo et al. (1989)	1998A&A...335..292E	Evans et al. (1998)
1989ApJ...336..822K	Knapp et al. (1989)	1998A&AS..130....1N	Neri et al. (1998)
1989ApJ...345L..87G	Gammie et al. (1989)	1998ApJ...509..392M	Meixner et al. (1998)
1989ApJ...346..201H	Huggins & Healy (1989)	1998ApJS..117..209K	Knapp et al. (1998)
1990A&A...228..503W	Woodsworth et al. (1990)	1999A&A...347..194O	Olofsson & Nyman (1999)
1990A&A...239..173H	Heske et al. (1990)	2000A&A...355...69P	Palla et al. (2000)
1990ApJ...358..251W	Wannier et al. (1990)	2001A&A...367..826J	Josselin & Lèbre (2001)
1991A&A...242..247B	Bujarrabal & Bachiller (1991)	2002A&A...390..501G	Groenewegen et al. (2002)
1991A&A...245..499A	Alcolea & Bujarrabal (1991)	2002ApJ...572..326B	Balser et al. (2002)
1991A&A...246..153L	Likkel et al. (1991)	2002ApJ...577..961H	Herpin et al. (2002)
1992A&A...256..235K	Kahane et al. (1992)	2003A&A...405..271M	Maas et al. (2003)
1992A&A...257..701B	Bujarrabal et al. (1992)	2004A&A...414..581H	Huggins et al. (2004)
1993A&A...267..515O	Omont et al. (1993)	2005A&A...429..977W	Woods et al. (2005)
1993A&A...269..231V	van der Veen et al. (1993)	2005ApJ...624..331H	Hrivnak & Biegging (2005)
1993A&A...273..185H	Hu et al. (1993)	2008A&A...488L..21H	He et al. (2008)
1993ApJ...402..292V	Volk et al. (1993)	2009ApJ...690..837M	Milam et al. (2009)
1994A&AS..103..301H	Hu et al. (1994)		

TABLE 7

OBSERVED PROPERTIES FROM LITERATURE FOR ALL THE 87 CONSIDERED POST-AGB STARS.

Object (or IRAS)	Other name	$F_{\text{CO2-1}}(\sigma)$ Jy MHz	NoteCO <sup>a</sup> km s <sup>-1</sup>	Vexp	F12 Jy	F25 Jy	F60 Jy	C12	C23	RCO25( $\sigma$ ) MHz
CRL 2688	EGG NEBULA	2220.96(964.73)		17.6						
HD 107369	CD-31 9638	(81.86) Tp								
V4334 Sgr	SAKURAI'S OBJECT	(11.63) Tp								
01005+7910		(6.00) Tp			3.905	24.23	10.07	1.98	-0.95	(0.248)
02143+5852	GLMP 26	(10.18)			5.897	18.06	5.395	1.22	-1.31	(0.564)
04166+5719	TW Cam	(6.00) Tp			8.252	5.602	1.84	-0.42	-1.21	(1.071)
04296+3429	GLMP 74	38.24		12.8	12.74	45.94	15.45	1.39	-1.18	0.832
04395+3601	CRL 618	1354.12(255.78)		16.7	470.8	1106.	1036.	0.93	-0.07	1.224(0.231)
04440+2605	RV Tau	(3.60)			22.52	18.05	6.502	-0.24	-1.11	(0.199)
05338-3051	RV Col	(81.86) Tp			0.349					
06034+1354	DY Ori	(3.60) Tp			12.43	14.89	4.182	0.20	-1.38	(0.242)
06072+0953	CT Ori	(4.80) Tp			6.145	5.545	1.24	-0.11	-1.63	(0.866)
06108+2743	SU Gem	(12.00)			7.905	5.684	2.193	-0.36	-1.03	(2.111)
06176-1036	Red Rectangle	40.25 (2.30)		4.9	421.6	456.1	173.1	0.09	-1.05	0.088(0.005)
06530-0213	PN PM 1-24	109.45 (25.12)		11.3	6.114	27.41	15.05	1.63	-0.65	3.993(0.916)
07134+1005	HD 56126	229.47 (61.58)		9.9	24.51	116.7	50.13	1.69	-0.92	1.966(0.528)
07284-0940	U Mon	(8.40)			124.3	88.43	26.59	-0.37	-1.30	(0.095)
07331+0021	AI Cmi	(6.72) Tp			15.32	68.11	18.51	1.62	-1.41	(0.099)
07399-1435	OH231.8+4.2	2248.50		21.4	18.98	226.3	548.3	2.69	0.96	9.936
07430+1115	GLMP 192	(9.45)			7.685	29.93	10.67	1.48	-1.12	(0.316)
08005-2356	V510 Pup	269.15		100.0	17.96	51.8	29.83	1.15	-0.60	5.196
08011-3627	AR Pup	(24.00) Tp			131.3	94.32	26.12	-0.36	-1.39	(0.254)
08187-1905	HD 70379	(13.08) Tp			0.714	17.62	12.31	3.48	-0.39	(0.742)
08544-4431	V390 Vel	40.37 (17.30)		5.6	180.3	158.8	56.25	-0.14	-1.13	0.254(0.109)
09032-3953	PN PM 2-9	128.81		25.0	20.38	125.9	92.31	1.98	-0.34	1.023
09370-4826	GLMP 255	(65.49) Tp			10.82	30.14	14.16	1.11	-0.82	(2.173)
09371+1212	FROSTY LEONIS	875.07 Tp		36.6		4.594	70.7		2.97	190.481
10158-2844	HR 4049	(4.80)			48.25	9.553	1.77	-1.76	-1.83	(0.502)
10178-5958	Hen 3-401	99.97		13.0	4.124	38.33	76.14	2.42	0.75	2.608
10194-5625	GLMP 271	(65.49) Tp			16.75	57.02	27.78	1.33	-0.78	(1.149)
10197-5750	Roberts 22	173.02		31.0	200.	1092.	588.3	1.84	-0.67	0.158
11000-6153	HD 95767	(81.86) Tp			22.13	15.65	10.9	-0.38	-0.39	(5.231)
11381-6401		(77.76) Tp			5.41	27.76	17.02	1.78	-0.53	(2.801)
11385-5517	HD 101584	793.98		45.0	92.6	138.3	193.	0.44	0.36	5.741
11544-6408	GLMP 315	(57.30) Tp			12.49	29.81	12.52	0.94	-0.94	(1.922)
12067-4508	HD 105578	(81.86) Tp			5.321	10.96	5.652	0.78	-0.72	(7.469)
12222-4652	HD 108015	(81.86) Tp			32.46	33.23	7.993	0.03	-1.55	(2.463)
12419-5414	Boomerang Nebula	184.84 (62.73)		25.5	4.173	5.502	13.65	0.30	0.99	33.595(11.401)
14488-5405	CPD -53 5736	39.80		15.0	6.587	63.74	30.54	2.46	-0.80	0.624
14524-6838	HD 131356	(81.86) Tp			13.23	10.26	4.107	-0.28	-0.99	(7.979)
15465+2818	R CrB	(55.70)			38.86	17.06	3.936	-0.89	-1.59	(3.265)
16342-3814	OH 344.1 +5.8	73.07 (4.78)		46.0	16.2	199.8	290.2	2.73	0.41	0.366(0.024)
16594-4656	WATER LILY NEBULA	626.73		14.0	44.92	298.	131.4	2.05	-0.89	2.103
17106-3046	PN PM 2-23	35.37		1.0	4.007	62.38	51.19	2.98	-0.21	0.567
17150-3224	RAFGL 6815	273.61 (26.76)		14.8	57.92	322.3	268.3	1.86	-0.20	0.849(0.083)
17245-3951	OH348.8-2.8	11.15		15.0	3.356	44.73	38.23	2.81	-0.17	0.249
17423-1755	Hen 3-1475	89.62 (2.82)		26.5	7.052	28.31	63.68	1.51	0.88	3.166(0.100)
17436+5003	V814 Her	180.62 (22.78)		11.5	6.122	183.5	151.7	3.69	-0.21	0.984(0.124)
17441-2411	AFGL 5385	139.76 (19.80)		12.5	42.78	191.1	106.5	1.63	-0.63	0.731(0.104)
17530-3348	AI Sco	10.15		2.8	17.59	11.38	2.95	-0.47	-1.47	0.892
17534+2603	89 Her	24.52 (1.41)		3.9	97.52	54.49	13.42	-0.63	-1.52	0.450(0.026)
18025-3906	PN PM 2-34	(53.21) Tp			4.295	41.2	30.11	2.45	-0.34	(1.292)
18095+2704	V887 Her	(3.60) Tp			45.09	125.7	27.83	1.11	-1.64	(0.029)
18276-1431	OH17.7-2.0	108.22 (5.64)		12.2	22.65	132.	120.	1.91	-0.10	0.820(0.043)
18281+2149	AC Her	3.38 (0.56)		1.5	41.43	65.33	21.37	0.49	-1.21	0.052(0.009)
18372-2257	V348 Sgr	(61.39) Tp			5.533	2.999	2.876	-0.66	-0.05	(20.470)
18415-2100	MV Sgr	(81.86) Tp			0.597	1.565	0.777	1.05	-0.76	(52.307)
19114+0002	AFGL 2343	837.39 (201.00)		31.5	31.33	648.3	515.9	3.29	-0.25	1.292(0.310)
19132-3336	RY Sgr	(122.78) Tp			77.17	26.25	5.433	-1.17	-1.71	(4.677)
19306+1407	GLMP 923	(9.24) Tp			3.584	58.65	31.83	3.03	-0.66	(0.158)
19343+2926	PN M1-92	319.13		32.5	17.52	59.76	118.4	1.33	0.74	5.340
19374+2359		(14.76) Tp			23.62	98.18	70.87	1.55	-0.35	(0.150)
19386+0155	V1648 Aql	(7.56) Tp			17.38	47.44	18.56	1.09	-1.02	(0.159)
19454+2920	GLMP 950	91.14 (18.24)		15.6	17.27	89.56	54.43	1.79	-0.54	1.018(0.204)
19475+3119	HD 331319	93.09 (15.45)		15.1	0.537	37.99	55.83	4.62	0.42	2.450(0.407)
19477+2401	CLOVERLEAF NEBULA	(7.27) Tp			11.24	54.92	27.13	1.72	-0.77	(0.132)
19480+2504	GLMP 953	88.65 (49.96)		17.5	20.81	67.89	43.16	1.28	-0.49	1.306(0.736)
19486+1350	TW Aql	(7.20) Tp				5.232	11.25		0.83	(1.376)
19500-1709	HD 187885	173.63 (53.58)		11.3	27.82	165.	73.4	1.93	-0.88	1.052(0.325)
19590-1249	LS IV -12 111	(12.36) Tp			0.293	10.26	6.45	3.86	-0.50	(1.205)
20000+3239	GLMP 963	53.36 (0.27)		12.2	15.03	70.97	29.99	1.69	-0.94	0.752(0.004)
20004+2955	V1027 Cyg	(6.00) Tp			31.72	36.96	4.656	0.17	-2.25	(0.162)
20028+3910	PN PM 2-43	88.11 (5.98)		14.5	41.78	210.8	143.1	1.76	-0.42	0.418(0.028)
20117+1634	R Sge	(12.00) Tp			10.6	7.543	2.123	-0.37	-1.38	(1.591)
20343+2625	V Vul	(3.60) Tp			12.35	5.688	1.294	-0.84	-1.61	(0.633)
20462+3416	LS II +34 26	(10.90) Tp			0.287	13.68	12.12	4.20	-0.13	(0.797)
20572+4919	V2324 Cyg	(10.18) Tp			4.335	10.97	9.696	1.01	-0.13	(0.928)
21537+6435	PN PM 1-334	(61.88) Tp			6.913	26.1	13.34	1.44	-0.73	(2.371)
22023+5249	GLMP 1051	(9.60) Tp			1.017	24.69	14.52	3.46	-0.58	(0.389)
22223+4327	V448 Lac	69.33		14.0	2.121	37.1	22.4	3.11	-0.55	1.869
22272+5435	HD 235858	490.04 (98.40)		10.1	73.88	302.4	96.59	1.53	-1.24	1.621(0.325)
22327-1731	HD213985	(8.40) Tp			5.569	4.664	2.107	-0.19	-0.86	(1.801)
22574+6609		64.29 (2.29)		19.8	9.003	29.47	20.64	1.29	-0.39	2.182(0.078)
23304+6147	PN PM 2-47	120.31 (20.61)		12.1	11.36	59.07	26.6	1.79	-0.87	2.037(0.349)

Refereed papers that contain original single dish observations of CO 2-1 line have been searched for in the ADS database using object position (with a search radius of  $1'$ ) for all 393 known pAGB stars in the version 2 of the Torun Catalog of pAGB stars (Szczerba et al. 2012). The search was done by Oct. 26, 2011. Both single pointing observations and single dish mapping are considered. Interferometer data are not considered due to the missing flux issue.

CO line parameters such as line peak temperature ( $T_{\text{mb}}$  or  $T_{\text{A}}^*$  or  $T_{\text{A}}'$ ), line area, line center velocity, and CSE expansion velocity are compiled, if available. The RMS noise level in the baseline are used as the  $1\sigma$  upper limit of undetected lines. The information about the telescopes, e.g., conversion factor to obtain main beam temperature from other antenna temperature scales, the telescope response (Jy/K) for conversion of main beam temperature into line flux (Jy), and the beam size of the telescopes at CO 2-1 line frequency are also collected. The telescope responses are adopted as nominal values for all involved telescopes: 7.33 Jy/K for the  $13''$  beam of the IRAM 30-m, 21 Jy/K for the  $22''$  beam of the JCMT 15-m, 25 Jy/K for the  $24''$  beam of the SEST 15-m, 44.4 Jy/K for the  $32''$  beam of the AROSMT 10-m, 39 Jy/K for the  $30''$  beam of both the NRAO 12-m and the CSO 10.4-m telescopes, and 29.4 Jy/K for the  $26''$  beam of the old 10-m Caltech OVRO telescope.

Here we give the list of all 175 CO 2-1 data records for 87 pAGB stars in Table 5, in which data records are sorted in increasing alphabetic order of object names and increasing observation dates. All the involved literature is collected in Table 6. When available, we also collect the information about the chemistry of the observed circumstellar shells (see Table 5).

Duplicated CO 2-1 observations were averaged to give a mean line strength. Before averaging, we convert all antenna temperature scales into velocity-integrated line flux in Jy MHz, so that the measured line strengths by different telescopes can be directly compared to check consistency. In the case when only line peak temperature was given in the papers, the line width  $V_{\text{exp}}$  is used to estimate the line area by assuming a Gaussian line profile. In very few cases when the  $V_{\text{exp}}$  is also not given, a fixed value of  $10 \text{ km s}^{-1}$  is assumed. The repeated observations usually agree with each other within a factor of 2-3, which is significantly larger than the usually accepted flux calibration uncertainty of 20 per cent. The reason of the large variation could be attributed to pointing error, bad weather, or technical problem during the observations. Weights are used in the averaging, which are set as follows: a weight of unity is set for most of the data entries, while a weight of 0.5 is given to those line area data estimated from line peak temperature and  $V_{\text{exp}}$ , and a weight of 2 is given to those single dish mapping data because these observations have less problems with pointing and are more reliable for nearby extended objects.

The average quantities for all the 87 pAGB objects (the velocity-integrated CO 2-1 line flux, and CSE expansion velocity  $V_{\text{exp}}$ ), as well as IRAS flux densities, IRAS colors (defined in Sect. 5.1), and CO-IR flux ratio  $R_{\text{CO25}}$  (defined by Eq. 1 in Sect. 3) are collected in Table 7.

## B. STATISTICAL PROPERTIES OF THE pAGB STAR SAMPLE

Statistical properties of the pAGB star sample are discussed here to assess if any selection effects would have biased the conclusions drawn from the sample. We discuss in this section the completeness of the

TABLE 7—*Continued*

Object (or IRAS)	Other name	$F_{\text{CO2-1}}(\sigma)$ Jy MHz	NoteCO <sup>a</sup> $\text{km s}^{-1}$	$V_{\text{exp}}$	F12 Jy	F25 Jy	F60 Jy	C12	C23	$R_{\text{CO25}}(\sigma)$ MHz
23321+6545	PN PM 2-48	218.78 (74.04)		16.1	13.66	85.61	63.96	1.99	-0.32	2.556( 0.865)
23541+7031	PK 118+08.1	142.61		54.0	91.36	92.28	55.7	0.01	-0.55	1.545
Z02229+6208		237.64		10.7						

NOTE.—The CO 2-1 line quantities are the average values from literature. New observations from this work are not included.

<sup>a</sup>'Tp' means the line area is estimated from line peak temperature and line width and thus is not as reliable as those values directly given in literature.

Torun Catalog of pAGB stars, our compilation of CO 2-1 observations, and the detection rates of CO 2-1 lines among the observed objects.

First of all, the Torun Catalog of pAGB stars was created with various object selection criteria (Szczerba et al. 2007). It is still unknown if the objects in this catalog are representative to all pAGB stars in the Galaxy. The version 2 of the catalog (Szczerba et al. 2012) is now divided into several sub-catalogs: likely, possible, RV Tau, R CrB/LTP/eHe, and unlikely. Here we plot the histograms of the Galactic position and *IRAS* 25 $\mu$ m flux densities of the three most important sub-catalogs: likely, RV Tau and R CrB/LTP/eHe, to check if the catalogs have any obvious bias. As shown in Fig. 8, all three sub-catalogs show decreasing trends from Galactic Center (GC) to anti-GC and from Galactic disc to high latitude and from 25 $\mu$ m-weak to 25 $\mu$ m-strong objects. Although the detailed comparison of these distributions with that of pAGB star model prediction for the Milky Way Galaxy is beyond the scope of this work, the trends roughly agree to the distribution of Galactic zero age main sequence stars. Thus, it is concluded that no severe bias can be seen in the three sub-catalogs from their Galactic position and IR flux density distributions.

Secondly, the pAGB stars with CO 2-1 observations in literature and in our survey (this work) are compared with all pAGB stars in the Torun Catalog in Fig. 9. The left and middle column of panels show that pAGB stars toward the GC and the Galactic disc have the lowest percentage of CO 2-1 observations, while most of the high Galactic latitude pAGB stars have been observed in CO 2-1 line. In the right column of Fig. 9, the CO observations of all three sub-groups of pAGB stars are clearly biased toward IR strong objects. Conversely, the CO observations of the R CrB/LTP/eHe types of pAGB stars in the third row of the figure are the most incomplete, because observers usually do not expect them to show CO line emission.

Thirdly, the detection rates of the CO 2-1 line among the ‘Likely’ and RV Tau type pAGB stars are plotted in Fig. 10. The R CrB/LTP/eHe type pAGB stars are not shown, because none of them have been detected in CO 2-1. Although there is no obvious trend along the Galactic longitude in the left panel of the figure, one can see in the middle panel that the CO 2-1 line detection rate in the Galactic disc is more than two times higher than at higher Galactic latitudes. This could be due to the higher masses of the pAGB stars in the Galactic disc, because more massive pAGB stars have thicker relic circumstellar envelope and thus have their CO lines more easily detected. In the right panel of the figure, there is a clear decreasing trend of CO 2-1 line detection rates toward IR-weaker objects, which indicates that the CO 2-1 line observations are sensitivity limited.

In a summary, the major bias effects found in the CO observations of pAGB stars are 1) pAGB stars in the GC direction are not adequately observed in CO 2-1 line; 2) The CO line observations in literature and our work are biased to IR-strong sources and are sensitivity limited. 3) The CO line observations of R CrB/LTP/eHe type pAGB stars are very incomplete in any sense;

## C. COMPARING AGB STARS ON THE CO-IR DIAGRAMS

Because this work is concentrated on pAGB stars, we only briefly mention some interesting points about the distribution of AGB stars and PNe on the new CO-IR diagram. Given below are more details not mentioned in Sect. 5.2.1 of the main text.

### C.1. O- and C-rich AGB stars

Although the majority of the O-rich AGB stars (empty blue circles in the second row of Fig. 3) concentrate in a small region on both the CO-IR and *IRAS* color-color diagrams, some objects do show significantly smaller  $R_{\text{CO}25}$  ratios (CO-weak) or significantly redder C23 colors. The redder objects could be either post-thermal pulse objects with detached CSEs (see, e.g., Steffen et al. 1998), OH/IR star candidates, or mis-identified pAGB stars. Many of the CO-weak objects are semi-regular variables of which the CSEs are probably optically thinner and thus CO molecules could have been partially destroyed by photodissociation.

The 28 OH/IR stars (half-shaded black circles) scatter in a larger region with similar or smaller CO-IR

flux ratios but redder C12 and C23 colors than the other O-rich AGB stars. This can be explained by cooler CO gas and lower average dust temperatures in the very thick CSEs of the OH/IR stars (Heske et al. 1990; Kastner 1992).

The O-rich AGB stars have slightly bluer C23 colors and about 3 times smaller  $R_{\text{CO}25}$  ratios than the C stars on average. The redder C23 color of C stars had been known (e.g., in the study of IRAS color-color diagram by van der Veen & Habing 1988) as due to the shallower emissivity of carbon rich dust in the 12-100  $\mu\text{m}$  region (Zuckerman & Dyck 1986b). The stronger CO line in C stars had long been recognized since the CO line survey of Nyman et al. (1992). The most possible explanation is higher CO abundance in carbon stars than in O-rich AGB stars, because only part of the oxygen atoms are used to make CO molecules in the latter.

## C.2. S stars against O- and C-rich AGB stars

S stars on the  $R_{\text{CO}25}$ -C23 diagram (red filled circles in the top row of Fig. 3) scatter in the similar regions as the C stars, indicating that the gas and dust properties of the CSE of S stars are closer to that of C stars than O-rich AGB stars. However, because S stars are expected to have much less dust in their CSEs due to the lock of most C and O atoms into gaseous CO molecules, their CO-IR flux ratios are intuitively expected to be even larger than that of typical C stars, which is not true in our Fig. 3. The not high enough CO-IR ratios of S stars could be explained by assuming that the CO molecules are not efficiently formed through ideal equilibrium chemistry (as discussed for C stars by Papoular 2008) and by assuming dust grains such as the recently proposed solid SiO dust (Wetzel et al. 2013) may still be efficiently formed around S stars.

Comparing the IRAS C-C diagrams in the upper right and middle right panels of Fig. 3, one can see that the S stars also have different IRAS colors than the C- and O-rich AGB stars. Their C12 colors are generally bluer than the latter, while their C23 colors are similar to C stars but redder than O-rich AGB stars. Again, the solid SiO dust proposed by Wetzel et al. (2013) has the potential to naturally explain these color differences. The solid SiO grains have the 10  $\mu\text{m}$  feature as normal silicates, but not the 18  $\mu\text{m}$  feature. Comparing with the Silicates dust in O-rich AGB stars, the lack of the 18  $\mu\text{m}$  feature of SiO dust in S stars just results in a weaker IRAS 25  $\mu\text{m}$  flux density, and thus bluer C12 and redder C23 colors of S stars than O-rich AGB stars, as showed above. Comparing with the C-rich dust in C stars, the most salient feature of the SiO dust is the appearance of the emission feature at 10  $\mu\text{m}$  which naturally causes the enhancement of the IRAS 12  $\mu\text{m}$  flux density, and thus bluer C12 and comparable C23 colors of the S stars against C stars.

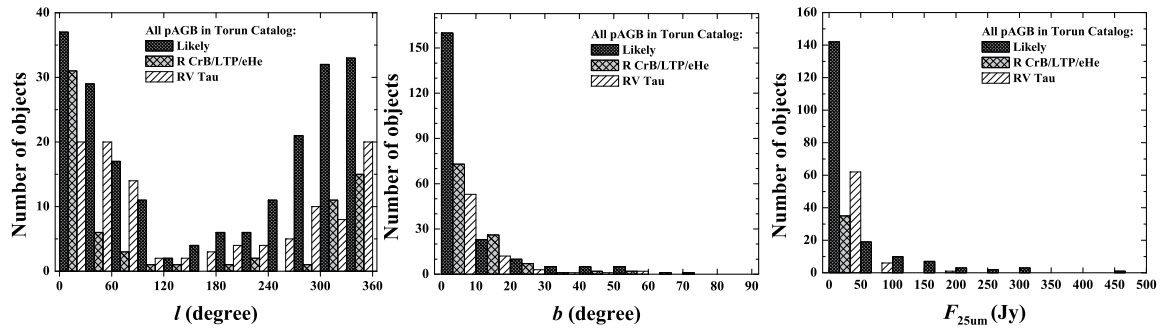


Fig. 8.— The histograms of the Galactic positions and *IRAS* 25  $\mu\text{m}$  flux density distributions of the pAGB stars in the Torun Catalog. Only the three most important sub-catalogs: Likely, R CrB/LTP/eHe, and RV Tau, are considered.

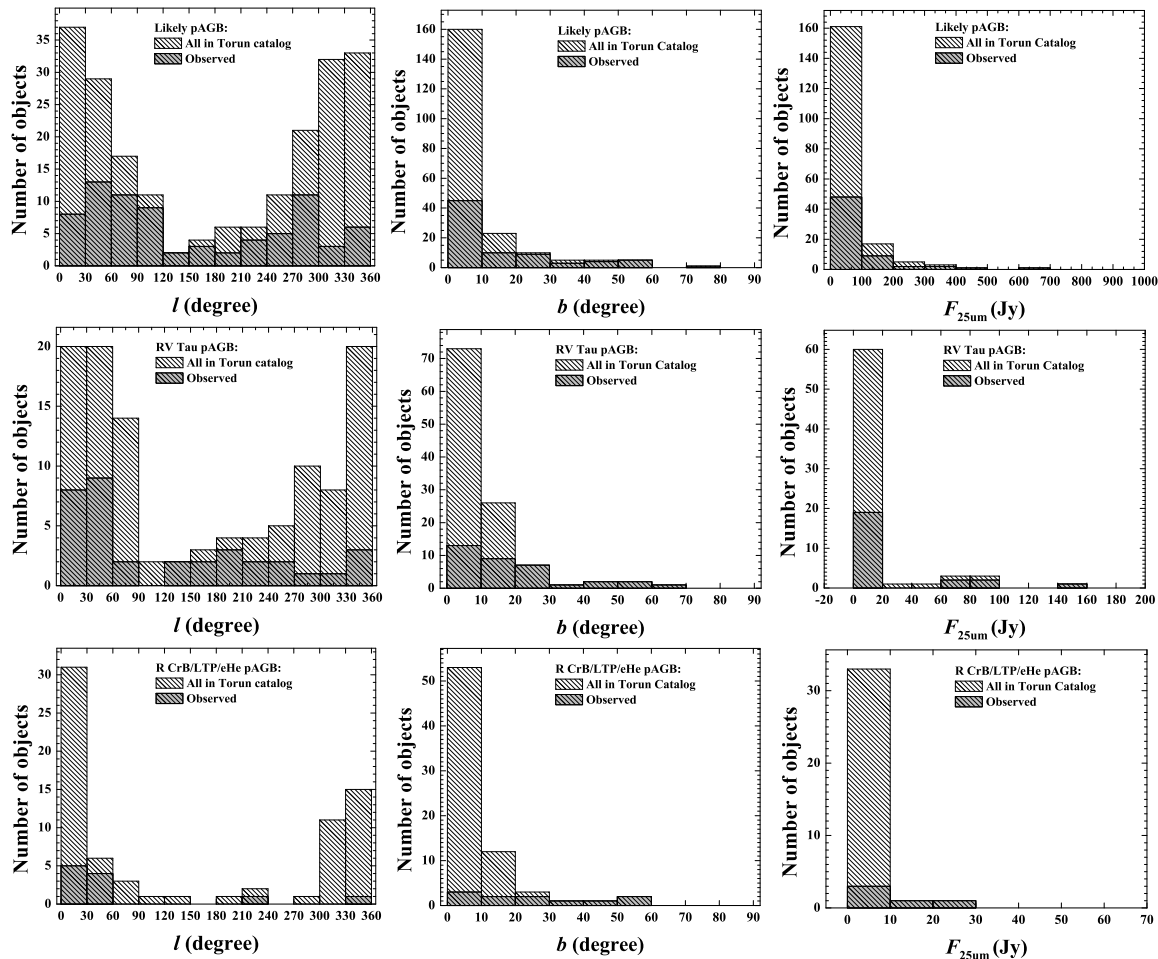


Fig. 9.— Comparison of the histograms of the pAGB stars observed in CO 2-1 with that of all pAGB stars in the Torun Catalog. Galactic positions and  $IRAS\ 25\ \mu\text{m}$  flux density distributions are shown in different columns of panels, while the three most important sub-groups of pAGB stars: Likely, R CrB/LTP/eHe, and RV Tau, are shown in different rows of panels.

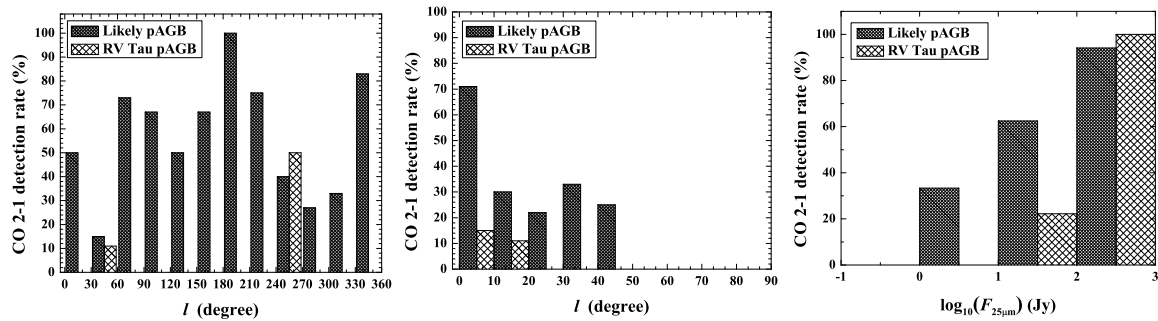


Fig. 10.— Comparison of the CO 2-1 line detection rates of ‘Likely’ and RV Tau type pAGB stars as a function of Galactic positions and *IRAS* 25  $\mu\text{m}$  flux densities.



## REFERENCES

- Alcolea, J., & Bujarrabal, V. 1991, *A&A*, 245, 499
- Alksnis, A., Balklavs, A., Dzervitis, U., Eglitis, I., Paupers, O., & Pundure, I. 2001, *Baltic Astronomy*, 10, 1
- Arhipova, V. P., Ikonnikova, N. P., Noskova, R. I., Sokol, G. V., Esipov, V. F., & Klochkova, V. G. 1999, *Astronomy Letters*, 25, 25
- Bachiller, R., Forveille, T., Huggins, P. J., & Cox, P. 1997, *A&A*, 324, 1123
- Bachiller, R., Gomez-Gonzalez, J., Bujarrabal, V., & Martin-Pintado, J. 1988, *A&A*, 196, L5
- Bakker, E. J., van Dishoeck, E. F., Waters, L. B. F. M., & Schoenmaker, T. 1997, *A&A*, 323, 469
- Balser, D. S., McMullin, J. P., & Wilson, T. L. 2002, *ApJ*, 572, 326
- Bujarrabal, V., Alcolea, J., & Planesas, P. 1992, *A&A*, 257, 701
- Bujarrabal, V., Alcolea, J., Van Winckel, H., Santander-García, M., & Castro-Carrizo, A. 2013, *A&A*, 557, A104
- Bujarrabal, V., & Bachiller, R. 1991, *A&A*, 242, 247
- Bujarrabal, V., Bachiller, R., Alcolea, J., & Martin-Pintado, J. 1988, *A&A*, 206, L17
- Bujarrabal, V., Castro-Carrizo, A., Alcolea, J., & Neri, R. 2005, *A&A*, 441, 1031
- Bujarrabal, V., Castro-Carrizo, A., Alcolea, J., & Sánchez Contreras, C. 2001, *A&A*, 377, 868
- Bujarrabal, V., van Winckel, H., Neri, R., Alcolea, J., Castro-Carrizo, A., & Deroo, P. 2007, *A&A*, 468, L45
- Şahin, T., Lambert, D. L., Klochkova, V. G., & Tavolganskaya, N. S. 2011, *MNRAS*, 410, 612
- Castro-Carrizo, A., Bujarrabal, V., Sánchez Contreras, C., Alcolea, J., & Neri, R. 2002, *A&A*, 386, 633
- Castro-Carrizo, A., Bujarrabal, V., Sánchez Contreras, C., Sahai, R., & Alcolea, J. 2005, *A&A*, 431, 979
- Castro-Carrizo, A., Neri, R., & Winters, J. M. 2004, in *Astronomical Society of the Pacific Conference Series*, Vol. 313, *Asymmetrical Planetary Nebulae III: Winds, Structure and the Thunderbird*, ed. M. Meixner, J. H. Kastner, B. Balick, & N. Soker, 314
- Castro-Carrizo, A., et al. 2010, *A&A*, 523, A59
- Cernicharo, J., Guélin, M., Penalver, J., Martin-Pintado, J., & Mauersberger, R. 1989, *A&A*, 222, L1
- Cerrigone, L., Hora, J. L., Umana, G., & Trigilio, C. 2009, *ApJ*, 703, 585
- Cox, P., Lucas, R., Huggins, P. J., Forveille, T., Bachiller, R., Guilloteau, S., Maillard, J. P., & Omont, A. 2000, *A&A*, 353, L25
- Dame, T. M., Hartmann, D., & Thaddeus, P. 2001, *ApJ*, 547, 792
- Dayal, A., & Bieging, J. H. 1996, *ApJ*, 472, 703
- de Ruyter, S., van Winckel, H., Dominik, C., Waters, L. B. F. M., & Dejonghe, H. 2005, *A&A*, 435, 161
- de Ruyter, S., van Winckel, H., Maas, T., Lloyd Evans, T., Waters, L. B. F. M., & Dejonghe, H. 2006, *A&A*, 448, 641
- Dougados, C., Rouan, D., Lacombe, F., Tiphene, D., & Forveille, T. 1990, *A&A*, 227, 437
- Eder, J., Lewis, B. M., & Terzian, Y. 1988, *ApJS*, 66, 183
- Evans, A., Eyres, S. P. S., Naylor, T., & Salama, A. 1998, *A&A*, 335, 292
- Forveille, T., Morris, M., Omont, A., & Likkell, L. 1987, *A&A*, 176, L13
- Gammie, C. F., Knapp, G. R., Young, K., Phillips, T. G., & Falgarone, E. 1989, *ApJL*, 345, L87
- Gérard, E., & Le Bertre, T. 2003, *A&A*, 397, L17
- Gielen, C., et al. 2011, *A&A*, 533, A99

- Giridhar, S., Lambert, D. L., Reddy, B. E., Gonzalez, G., & Yong, D. 2005, *ApJ*, 627, 432
- Greaves, J. S., & Holland, W. S. 1997, *A&A*, 327, 342
- Groenewegen, M. A. T., Sevenster, M., Spoon, H. W. W., & Pérez, I. 2002, *A&A*, 390, 501
- Hajian, A. R., Phillips, J. A., & Terzian, Y. 1996, *ApJ*, 467, 341
- He, J. H., Imai, H., Hasegawa, T. I., Campbell, S. W., & Nakashima, J. 2008, *A&A*, 488, L21
- Herpin, F., Goicoechea, J. R., Pardo, J. R., & Cernicharo, J. 2002, *ApJ*, 577, 961
- Heske, A., Forveille, T., Omont, A., van der Veen, W. E. C. J., & Habing, H. J. 1990, *A&A*, 239, 173
- Hodge, T. M., Kraemer, K. E., Price, S. D., & Walker, H. J. 2004, *ApJS*, 151, 299
- Hony, S., Waters, L. B. F. M., & Tielens, A. G. G. M. 2002, *A&A*, 390, 533
- Hrivnak, B. J., & Bieging, J. H. 2005, *ApJ*, 624, 331
- Hrivnak, B. J., Lu, W., Maupin, R. E., & Spitzbart, B. D. 2010, *ApJ*, 709, 1042
- Hu, J. Y., Slijkhuis, S., Nguyen-Q-Rieu, & de Jong, T. 1993, *A&A*, 273, 185
- Hu, J. Y., te Lintel Hekkert, P., Slijkhuis, F., Baas, F., Sahai, R., & Wood, P. R. 1994, *A&AS*, 103, 301
- Huggins, P. J., Bachiller, R., Cox, P., & Forveille, T. 1996, *A&A*, 315, 284
- Huggins, P. J., Bachiller, R., Planesas, P., Forveille, T., & Cox, P. 2005, *ApJS*, 160, 272
- Huggins, P. J., & Healy, A. P. 1989, *ApJ*, 346, 201
- Huggins, P. J., Muthu, C., Bachiller, R., Forveille, T., & Cox, P. 2004, *A&A*, 414, 581
- Jorissen, A., & Knapp, G. R. 1998, *A&AS*, 129, 363
- Josselin, E., & Lèbre, A. 2001, *A&A*, 367, 826
- Jura, M. 1986, *ApJ*, 309, 732
- Jura, M., Balm, S. P., & Kahane, C. 1995, *ApJ*, 453, 721
- Kahane, C., Cernicharo, J., Gomez-Gonzalez, J., & Guelin, M. 1992, *A&A*, 256, 235
- Kastner, J. H. 1992, *ApJ*, 401, 337
- Kawabe, R., et al. 1987, *ApJ*, 314, 322
- Kerschbaum, F., & Olofsson, H. 1999, *A&AS*, 138, 299
- Knapp, G. R., Phillips, T. G., Leighton, R. B., Lo, K. Y., Wannier, P. G., Wootten, H. A., & Huggins, P. J. 1982, *ApJ*, 252, 616
- Knapp, G. R., Young, K., Lee, E., & Jorissen, A. 1998, *ApJS*, 117, 209
- Knapp, G. R., et al. 1989, *ApJ*, 336, 822
- Kwok, S. 1993, *ARA&A*, 31, 63
- Kwok, S., Boreiko, R. T., & Hrivnak, B. J. 1987, *ApJ*, 312, 303
- Kwok, S., Volk, K. M., & Hrivnak, B. J. 1989, *ApJ*, 345, L51
- Libert, Y., Winters, J. M., Le Bertre, T., Gérard, E., & Matthews, L. D. 2010, *A&A*, 515, A112
- Likkel, L. 1989, *ApJ*, 344, 350
- Likkel, L., Forveille, T., Omont, A., & Morris, M. 1991, *A&A*, 246, 153
- Likkel, L., & Morris, M. 1988, *ApJ*, 329, 914
- Loup, C., Forveille, T., Omont, A., & Paul, J. F. 1993, *A&AS*, 99, 291
- Maas, T., Van Winckel, H., Lloyd Evans, T., Nyman, L.-Å., Kilkenny, D., Martinez, P., Marang, F., & van Wyk, F. 2003, *A&A*, 405, 271
- Mamon, G. A., Glassgold, A. E., & Huggins, P. J. 1988, *ApJ*, 328, 797
- Manteiga, M., García-Hernández, D. A., Ulla, A., Manchado, A., & García-Lario, P. 2011, *AJ*, 141, 80

- Meixner, M., Campbell, M. T., Welch, W. J., & Likkell, L. 1998, *ApJ*, 509, 392
- Men'shchikov, A. B., Schertl, D., Tuthill, P. G., Weigelt, G., & Yungelson, L. R. 2002, *A&A*, 393, 867
- Milam, S. N., Woolf, N. J., & Ziurys, L. M. 2009, *ApJ*, 690, 837
- Morris, M., & Bowers, P. F. 1980, *AJ*, 85, 724
- Murakawa, K., Ohnaka, K., Driebe, T., Hofmann, K., Oya, S., Schertl, D., & Weigelt, G. 2008, *A&A*, 489, 195
- Neri, R., Kahane, C., Lucas, R., Bujarrabal, V., & Loup, C. 1998, *A&AS*, 130, 1
- Nyman, L.-Å., et al. 1992, *A&AS*, 93, 121
- Olofsson, H., & Nyman, L.-Å. 1999, *A&A*, 347, 194
- Omont, A., Loup, C., Forveille, T., te Lintel Hekkert, P., Habing, H., & Sivagnanam, P. 1993, *A&A*, 267, 515
- Palla, F., Bachiller, R., Stanghellini, L., Tosi, M., & Galli, D. 2000, *A&A*, 355, 69
- Papoular, R. 2008, *MNRAS*, 390, 1727
- Parthasarathy, M., García-Lario, P., Gauba, G., de Martino, D., Nakada, Y., Fujii, T., Pottasch, S. R., & San Fernández de Córdoba, L. 2001, *A&A*, 376, 941
- Peeters, E., Hony, S., Van Kerckhoven, C., Tielens, A. G. G. M., Allamandola, L. J., Hudgins, D. M., & Bauschlicher, C. W. 2002, *A&A*, 390, 1089
- Pereira, C. B., Lorenz-Martins, S., & Machado, M. 2004, *A&A*, 422, 637
- Pereira, C. B., & Miranda, L. F. 2007, *A&A*, 462, 231
- Piovan, L., Tantaló, R., & Chiosi, C. 2003, *A&A*, 408, 559
- Preston, G. W., Krzeminski, W., Smak, J., & Williams, J. A. 1963, *ApJ*, 137, 401
- Ramstedt, S., Schöier, F. L., & Olofsson, H. 2009, *A&A*, 499, 515
- Rao, S. S., Giridhar, S., & Lambert, D. L. 2012, *MNRAS*, 419, 1254
- Roberts, M. S. 1962, *AJ*, 67, 79
- Roddier, F., Roddier, C., Graves, J. E., & Northcott, M. J. 1995, *ApJ*, 443, 249
- Ryans, R. S. I., Dufton, P. L., Mooney, C. J., Rolleston, W. R. J., Keenan, F. P., Hubeny, I., & Lanz, T. 2003, *A&A*, 401, 1119
- Sahai, R., Bujarrabal, V., Castro-Carrizo, A., & Zijlstra, A. 2000, *A&A*, 360, L9
- Sahai, R., & Nyman, L.-Å. 1997, *ApJL*, 487, L155
- Sánchez Contreras, C., Bujarrabal, V., & Alcolea, J. 1997, *A&A*, 327, 689
- Sánchez Contreras, C., Bujarrabal, V., Castro-Carrizo, A., Alcolea, J., & Sargent, A. 2004, *ApJ*, 617, 1142
- Sánchez Contreras, C., Cortijo-Ferrero, C., Miranda, L. F., Castro-Carrizo, A., & Bujarrabal, V. 2010, *ApJ*, 715, 143
- Sánchez Contreras, C., Sahai, R., Gil de Paz, A., & Goodrich, R. 2008, *ApJS*, 179, 166
- Seaquist, E. R., Plume, R., & Davis, L. E. 1991, *ApJ*, 367, 200
- Sevenster, M. N. 2002, *AJ*, 123, 2772
- Silva, A. M., Azcarate, I. N., Poppel, W. G. L., & Likkell, L. 1993, *A&A*, 275, 510
- Slijkhuis, S., de Jong, T., & Hu, J. Y. 1991, *A&A*, 248, 547
- Stasińska, G., Szczerba, R., Schmidt, M., & Siódmiak, N. 2006, *A&A*, 450, 701
- Steffen, M., Szczerba, R., & Schoenberner, D. 1998, *A&A*, 337, 149
- Stephenson, C. B. 1989, *Publications of the Warner & Swasey Observatory*, 3, 53
- Suárez, O., García-Lario, P., Manchado, A., Man-teiga, M., Ulla, A., & Pottasch, S. R. 2006, *A&A*, 458, 173

- Szczerba, R., & Marten, H. 1993, in European Southern Observatory Conference and Workshop Proceedings, Vol. 46, European Southern Observatory Conference and Workshop Proceedings, ed. H. E. Schwarz, 90
- Szczerba, R., Siódmiak, N., Stasińska, G., & Borkowski, J. 2007, *A&A*, 469, 799
- Szczerba, R., Siódmiak, N., Stasińska, G., Borkowski, J., García-Lario, P., Suárez, O., Hajduk, M., & García-Hernández, D. A. 2012, in IAU Symposium, Vol. 283, IAU Symposium, 506–507
- te Lintel Hekkert, P. 1991, *A&A*, 248, 209
- te Lintel Hekkert, P., & Chapman, J. M. 1996, *A&AS*, 119, 459
- te Lintel Hekkert, P. T. L., Chapman, J. M., & Zijlstra, A. A. 1992, *ApJ*, 390, L23
- van der Veen, W. E. C. J., & Habing, H. J. 1988, *A&A*, 194, 125
- van der Veen, W. E. C. J., Habing, H. J., & Geballe, T. R. 1989, *A&A*, 226, 108
- van der Veen, W. E. C. J., Trams, N. R., & Waters, L. B. F. M. 1993, *A&A*, 269, 231
- van Winckel, H. 2003, *ARA&A*, 41, 391
- van Winckel, H., Lloyd Evans, T., Briquet, M., De Cat, P., Degroote, P., De Meester, W., De Ridder, J., & et al. 2009, *A&A*, 505, 1221
- Van Winckel, H., & Reyniers, M. 2000, *A&A*, 354, 135
- Vandenbussche, B., et al. 2002, *A&A*, 390, 1033
- Volk, K., & Kwok, S. 1987, *ApJ*, 315, 654
- Volk, K., Kwok, S., & Woodsworth, A. W. 1993, *ApJ*, 402, 292
- Wannier, P. G., Leighton, R. B., Knapp, G. R., Redman, R. O., Phillips, T. G., & Huggins, P. J. 1979, *ApJ*, 230, 149
- Wannier, P. G., & Sahai, R. 1987, *ApJ*, 319, 367
- Wannier, P. G., Sahai, R., Andersson, B.-G., & Johnson, H. R. 1990, *ApJ*, 358, 251
- Waters, L. B. F. M., et al. 1998, *Nature*, 391, 868
- Wetzel, S., Klevenz, M., Gail, H.-P., Pucci, A., & Trieloff, M. 2013, *A&A*, 553, A92
- Winters, J. M., Le Bertre, T., Jeong, K. S., Nyman, L., & Epchtein, N. 2003, *A&A*, 409, 715
- Winters, J. M., Le Bertre, T., Pety, J., & Neri, R. 2007, *A&A*, 475, 559
- Witt, A. N., Vijh, U. P., Hobbs, L. M., Aufdenberg, J. P., Thorburn, J. A., & York, D. G. 2009, *ApJ*, 693, 1946
- Woods, P. M., Nyman, L., Schöier, F. L., Zijlstra, A. A., Millar, T. J., & Olofsson, H. 2005, *A&A*, 429, 977
- Woodsworth, A. W., Kwok, S., & Chan, S. J. 1990, *A&A*, 228, 503
- Zijlstra, A. A. 2007, *Baltic Astronomy*, 16, 79
- Zuckerman, B., & Dyck, H. M. 1986a, *ApJ*, 304, 394
- . 1986b, *ApJ*, 311, 345
- . 1989, *A&A*, 209, 119